

Evaluation of the MACC operational forecast system- potential and challenges of global near-real-time modelling with respect to reactive gases in the troposphere

A. Wagner¹, A.-M. Blechschmidt², I. Bouarar^{3[*]}, E.-G. Brunke⁴, C. Clerbaux³,
M. Cupeiro⁵, P. Cristofanelli⁶, H. Eskes⁷, J. Flemming⁸, H. Flentje¹, M.
George³, S. Gilge¹, A. Hilboll², A. Inness⁸, J. Kapsomenakis⁹, A. Richter², L.
Ries¹⁰, W. Spangl¹¹, O. Stein¹², R. Weller¹³, C. Zerefos⁹

[1]{Deutscher Wetterdienst, Meteorologisches Observatorium Hohenpeissenberg, Germany}

[2]{Institute of Environmental Physics, University of Bremen, Germany}

[3]{Sorbonne Universités, UPMC Univ. Paris 06; Université Versailles St-Quentin;
CNRS/INSU, LATMOS-IPSL, Paris, France}

[4]{South African Weather Service, Stellenbosch, South Africa}

[5]{National Meteorological Service, Ushuaia, Tierra del Fuego, Argentina}

[6]{National Research Council of Italy, ISAC, Bologna, Italy}

[7]{Royal Netherlands Meteorological Institute, De Bilt, The Netherlands}

[8]{European Centre for Medium-range Weather Forecasts, Reading, UK}

[9]{Academy of Athens, Research Centre for Atmospheric Physics and Climatology, Athens,
Greece}

[10]{Federal Environment Agency, GAW Global Station Zugspitze/Hohenpeissenberg,
Zugspitze 5, D-82475 Zugspitze}

[11]{Umweltbundesamt GmbH, Air Pollution Control & Climate Change Mitigation, Vienna,
Austria}

[12]{Forschungszentrum Jülich, IEK-8 (Troposphere), Jülich, Germany}

[13]{Alfred Wegener Institute, Bremerhaven, Germany}

[*]{now at: Max-Planck-Institut for Meteorology, Hamburg, Germany}

Correspondence to: A. Wagner (Annette.wagner@dwd.de)

Abstract

Monitoring Atmospheric Composition and Climate (MACC) represented the European Union's Copernicus Atmosphere Monitoring Service (CAMS) (<http://www.copernicus.eu/>), which became fully operational in the course of 2015. The global near-real-time MACC model production run for aerosol and reactive gases provides daily analyses and 5-day forecasts of atmospheric composition fields. It is the only assimilation system world-wide that is operational to produce global analyses and forecasts of reactive gases and aerosol fields. We have investigated the ability of the MACC analysis system to simulate tropospheric concentrations of reactive gases (CO, O₃, and NO₂) covering the period between 2009 and 2012. A validation was performed based on CO, NO₂ and O₃ surface observations from the Global Atmosphere Watch (GAW) network, O₃ surface observations from the European Monitoring and Evaluation Programme (EMEP) and furthermore, NO₂ tropospheric columns, as well as CO total columns derived from satellite sensors. The MACC system proved capable of reproducing reactive gas concentrations in consistent quality, however, with a seasonally dependent bias compared to surface and satellite observations: For northern hemisphere surface O₃ mixing ratios, positive biases appear during the warm seasons and negative biases during the cold parts of the years, with monthly Modified Normalised Mean Biases (MNMBs) ranging between -30% and 30% at the surface. Model biases are likely to result from difficulties in the simulation of vertical mixing at night and deficiencies in the model's dry deposition parameterization. Observed tropospheric columns of NO₂ and CO could be reproduced correctly during the warm seasons, but are mostly underestimated by the model during the cold seasons, when anthropogenic emissions are at a highest, especially over the US, Europe and Asia. Monthly MNMBs of the satellite data evaluation range between -110% and 40% for NO₂ and at most -20% for CO, over the investigated regions. The underestimation is likely to result from a combination of errors concerning the dry deposition parameterization and certain limitations in the current emission inventories, together with an insufficiently established seasonality in the emissions.

1 Introduction

The impact of reactive gases on climate, human health and the environment has gained increasing public and scientific interest in the last decade (Bell et al., 2006; Cape 2008; Mohnen et al., 2013; Seinfeld and Pandis 2006; Selin et al., 2009) as air pollutants such as carbon monoxide (CO), nitrogen oxides (NO_x) and ozone (O₃) are known to have acute and chronic effects on human health, ranging from minor upper respiratory irritation to chronic respiratory and heart disease, lung cancer, acute respiratory infections in children and chronic bronchitis in adults (Bell et al., 2006; Kampa and Castanas 2006). Tropospheric ozone, even in small concentrations, is also known to cause plant damage in reducing plant primary productivity as well as crop yields (e.g. Ashmore 2005). It is also contributing to global warming by direct and indirect radiative forcing (Forster et al., 2007, Sitch et al., 2007). Pollution events can be caused by local sources and processes but are also influenced by continental and intercontinental transport of air masses. Global models can provide the transport patterns of air masses and deliver the boundary conditions for regional models, facilitating the forecast and investigation of air pollutants.

The European Union (EU)-funded research project MACC (consisting of a series of European projects, MACC to MACC-III), provides the preparatory work that will form the basis of the Copernicus Atmosphere Monitoring Service. This service is established by the EU to provide a range of products of societal and environmental value with the aim to help European governments respond to climate change and air quality problems. MACC provides reanalysis, monitoring products of atmospheric key constituents (e.g. Inness et al., 2013), as well as operational daily forecasting of greenhouse gases, aerosols and reactive gases (Benedetti et al., 2011; Stein et al., 2012) on a global and on European-scale level, and derived products such as solar radiation. An important aim of the MACC system is to describe the occurrence, magnitude and transport pathways of disruptive events, e.g., volcanoes (Flemming and Inness, 2013), major fires (Huijnen et al., 2012; Kaiser et al., 2012) and dust storms (Cuevas et al., 2015). The product catalogue can be found on the MACC website, <http://copernicus-atmosphere.eu>. For the generation of atmospheric products, state-of-the-art atmospheric modelling is combined with assimilated satellite data (Hollingsworth et al., 2008, Inness et al., 2013, 2015, more general information about data assimilation can be found in e.g. Ballabrera-Poy et al., 2009 or Kalnay 2003). Within the MACC project there is a dedicated validation

activity to provide up-to-date information on the quality of the reanalysis, daily analyses and forecasts. Validation reports are updated regularly and are available on the MACC websites.

The MACC global near-real-time (NRT) production model for reactive gases and aerosol has operated with data assimilation from September 2009 onwards, providing boundary conditions for the MACC regional air quality products (RAQ), and other downstream users. The model simulations also provide input for the stratospheric ozone analyses delivered in near-real-time by the MACC stratospheric ozone system (Lefever et al., 2014).

In this paper we describe the investigation of the potential and challenges of near-real-time modelling with the MACC analysis system between 2009 and 2012. We concentrate on this period because of the availability of validated independent observations, namely surface observations from the Global Atmosphere Watch Programme GAW, the European Monitoring and Evaluation Programme EMEP, as well as total column/tropospheric column satellite data from the MOPITT (Measurement Of Pollution In The Troposphere), SCIAMACHY (SCanning Imaging Absorption spectroMeter for Atmospheric CHartographY) and GOME-2 (Global Ozone Monitoring Experiment-2) sensors that are used for comparison. In particular, we study the model's ability to reproduce the seasonality and absolute values of CO and NO₂ in the troposphere as well as NO₂, O₃ and CO at the surface. The impact of changes in model version, data assimilation and emission inventories on the model performance is examined and discussed. The paper is structured in the following way: Section 2 contains a description of the model and the validation data sets as well as the applied validation metrics. Section 3 presents the validation results for CO, NO₂ and O₃. Section 4 provides the discussion and section 5 the conclusions of the paper.

2 Data and methods

2.1 The MACC model system in the 2009-2012 period

The MACC global products for reactive gases consist of a reanalysis performed for the years 2003-2012 (Inness et al., 2013) and the near-real-time analysis and forecast, largely based on the same assimilation and forecasting system, but targeting different user groups. The Model for OZone And Related chemical Tracers (MOZART) chemical transport model (CTM) is coupled to the Integrated Forecast System (IFS) of the European Centre for Medium-Range Weather forecast (ECMWF), which together represent the MOZART-IFS model system (Flemming et al., 2009 and Stein et al. 2012). An alternative analysis system has been set up

1 based on the global chemistry Transport Model version 5 (TM5, see also Huijnen et al.,
2 2010). Details of the MOZART version used in the MACC global products can be found in
3 Kinnison et al., 2007 and Stein et al. (2011, 2012). In the simulation, the IFS and the
4 MOZART model run in parallel and exchange several two- and three-dimensional fields
5 every model hour using the Ocean Atmosphere Sea Ice Soil version 4 (OASIS4) coupling
6 software (Valcke and Redler 2006), thereby producing three-dimensional IFS fields for O₃,
7 CO, SO₂, NO_x, HCHO, sea salt aerosol, desert dust, black carbon, organic matter, and total
8 aerosol. The IFS provides meteorological data to MOZART. Data assimilation and transport
9 of the MACC species takes place in IFS, while the whole chemical reaction system is
10 calculated in MOZART.

11 The MACC_osuite (operational suite) is the global near-real-time MACC model production
12 run for aerosol and reactive gases. Here, we have investigated only the MACC analysis. In
13 contrast to the reanalysis, the MACC_osuite is a near-real-time run, which implies that it is
14 only run once in near-real-time and may thus contain inconsistencies in e.g. the assimilated
15 data. The MACC_osuite was based on the IFS cycle CY36R1 with IFS model resolution of
16 approximately 100 km by 100 km at 60 levels (T159L60) from September 2009 until July
17 2012. The gas-phase chemistry module in this cycle is based on MOZART version 3.0
18 (Kinnison et al., 2007). The model has been upgraded, following updates of the ECMWF
19 meteorological model and MACC-specific updates, i.e. in chemical data assimilation and with
20 respect to the chemical model itself. Thus, from July 2012 onwards, the MACC_osuite has
21 run with a change of the meteorological model to a new IFS cycle (version CY37R3), with an
22 IFS model resolution of approximately 80 km at 60 levels (T255L60) and an upgrade of the
23 MOZART version 3.5 (Kinnison et al., 2007; Emmons et al., 2011; Stein et al. 2013). This
24 includes, amongst others, updated velocity fields for the dry deposition of O₃ over ice, as
25 described in Stein et al. (2013). A detailed documentation of system changes can be found at:

26 http://www.copernicus-atmosphere.eu/oper_info/nrt_info_for_users/

27 **2.1.1 Emission inventories and assimilated data sets**

28 In the MACC_osuite, anthropogenic emissions are based on emissions from the EU project
29 REanalysis of the TRopospheric chemical composition Over the past 40 years (RETRO) merged
30 with updated emissions for East Asia from the Regional Emission inventory in ASia (REAS)
31 inventory, (Schultz et al. 2007) in the following referred to as RETRO-REAS. The horizontal

1 resolution is 0.5° in latitude and longitude and it contains a monthly temporal resolution.
2 Biogenic emissions are taken from Global Emissions Initiative (GEIA), fire emissions are
3 based on a climatology derived from Global Fire Emissions Database version 2 (GFEDv2,
4 van der Werf et al., 2006) until April 2010, when fire emissions change to Global Fire
5 Assimilation System (GFAS) emissions (Kaiser et al., 2012). Between January 2011 and
6 October 2011 there has been a fire emission reading error in the model, where, instead of
7 adjusting emissions to the appropriate month, the same set of emissions have been read
8 throughout this period.

9 After the model upgrade to the new cycle version CY37R3, in July 2012, the emission
10 inventories changed from the merged RETRO-REAS and GEIA inventories, used in the
11 previous cycle, to the MACCity anthropogenic and biogenic emissions (Granier et al., 2011)
12 and (climatological) Model of Emissions of Gases and Aerosols from Nature version 2
13 (MEGAN-v2, see Guenther et al., 2006) emission inventories. Wintertime anthropogenic CO
14 emissions are scaled up over Europe and North America (see Stein et al., 2014). Near-real-
15 time fire emissions are taken from GFASv1.0 (Kaiser et al. 2012), for both gas-phase and
16 aerosol.

17 In the MACC_osuite, the initial conditions for some of the chemical species are provided by
18 data assimilation of atmospheric composition observations from satellites (see Benedetti et
19 al., 2009, Inness et al., 2009, 2013, Massart et al., 2014). Table 1 lists the assimilated data
20 products. From September 2009 to June 2012, O_3 total columns of the Microwave Limb
21 Sounder (MLS) and Solar Backscatter Ultraviolet (SBUV-2) instruments are assimilated, as
22 well as Ozone Monitoring Instrument (OMI) and SCIAMACHY total columns (the latter only
23 until March 2012, when the European Space Agency lost contact with the ENVironmental
24 SATellite ENVISAT). CO total columns are assimilated from the Infrared Atmospheric
25 Sounding Interferometer (IASI) sensor and aerosol total optical depth is assimilated from the
26 Moderate Resolution Imaging Spectroradiometer (MODIS) instrument. After the model cycle
27 update in July 2012, data assimilation also contains OMI tropospheric columns of NO_2 and
28 SO_2 , as well as CO MOPITT total columns. The CO total columns retrieved by MOPITT and
29 IASI instruments have a relatively similar seasonality, but there is a systematic difference
30 with MOPITT CO being higher over most regions in the northern hemisphere, especially
31 during winter and spring. George et al. (2015) investigated the differences between MOPITT
32 and IASI, and showed the impact of a priori information on the retrieved measurements.

Table 1 and 2 summarize the data assimilation and setup of the MACC_osuite.

2.2 Validation data and methodology

In this study, mainly the same evaluation data sets have been used as during the MACC near-real-time validation exercise. This implies some discontinuities in the evaluations, e.g. the substitution of SCIAMACHY data with GOME-2 data after the loss of the ENVISAT sensor or an exclusion of MOPITT satellite data after the start of its assimilation into the model. The continuous process of updating and complementation of data sets in databases requires the selection and definition of an evaluation data set at some point. The comparatively small inconsistencies between our data sets are considered to have a negligible impact on the overall evaluation results.

2.2.1 GAW surface O₃, CO and NO₂ observations

The Global Atmosphere Watch (GAW) programme of the World Meteorological Organization (WMO) has been established to provide reliable long-term observations of the chemical composition and physical properties of the atmosphere, which are relevant for understanding atmospheric chemistry and climate change (WMO, 2013). GAW tropospheric O₃ measurements are performed in a way to be suitable for the detection of long-term regional and global changes. Furthermore, the GAW measurement programme focuses on observations, which are regionally representative and should be free from influence of significant local pollution sources and suited for the validation of global chemistry climate models (WMO 2007). Detailed information on GAW and GAW related O₃, CO and NO₂ measurements can be found in WMO (2010, 2011 and 2013).

Hourly O₃, CO and NO₂ data have been downloaded from the WMO/GAW World Data Centre for Greenhouse Gases (WDCGG) for the period between 09/2009 and 12/2012 (status of download: 07/2013). Our evaluation includes 6 stations with surface observations for NO₂, 29 stations for CO and 50 stations with surface observations for O₃. Table 3 lists the geographic coordinates and altitudes of the individual stations. Being a long-term data network, the data in the database are provided with a temporal delay of approximately 2 years. As the data in the database become sparse towards the end of the validation period, near-real-time observations, as used in the MACC-project for near-real-time validation, presented on the MACC website, have been included to complement the validation data sets. For the detection of long-term trends and year-to-year variability, the data quality objectives (DQOs) for CO in

GAW measurements are set to a maximum uncertainty of ± 2 ppb and to ± 5 ppb for marine boundary layer sites and continental sites that are influenced by regional pollution and to ± 1 ppb for ozone (WMO, 2012, 2013) and 0.08 ppb for NO₂ (WMO 2011).

For the evaluation with GAW station data, 6-hourly values (0, 6, 12, 18 UTC) of the analysis mode have been extracted from the model and are matched with hourly observational GAW station data. Model mixing ratios at the stations' location have been linearly interpolated from the model data in the horizontal. In the vertical, modelled gas mixing ratios have been extracted at the model level, which is closest to the GAW stations' altitude. Validation scores (see section 2.3) have been calculated for each station between the 6-hourly model analysis data and the corresponding observational data for the entire period (09/2009- 12/2012) and as monthly averages.

2.2.2 EMEP surface O₃ observations

The European Monitoring and Evaluation Programme (EMEP) is a scientifically based and policy driven programme under the Convention on Long-Range Transboundary Air Pollution (CLRTAP) for international co-operation to solve transboundary air pollution problems. Measurements of air quality in Europe have been carried out under the EMEP since 1977.

A detailed description of the EMEP measurement programme can be found in Tørseth et al. (2012). The surface hourly ozone data between 09/2009 and 12/2012 have been downloaded from the EMEP data web-page (<http://www.nilu.no/projects/ccc/emepdata.html>). For the validation, only stations meeting the 75% availability threshold per day and per month are taken into account. The precision is close to 1.5 ppb for a 10s measurement. More information about the ozone data quality, calibration and maintenance procedures can be found in Aas et al. (2000).

For comparison with EMEP data, 3-hourly model values (0, 3, 6, 12, 15, 18, 21 UTC) of the analysis mode have been chosen. We used this data set to test the dependency of the biases on day and night time basis, separately. Gas mixing ratios have been extracted from the model and are matched with hourly observational surface ozone data at 124 EMEP stations in the same way as for the GAW station data. The EMEP surface ozone values and the interpolated surface modeled values are compared on a monthly basis for the latitude bands of 30°N – 40°N (southern Europe), 40°N – 50°N (central Europe) and 50°N – 70°N (northern Europe). For the identification of differences in the MACC_osuite performance between day and night time, the MACC_osuite simulations and the EMEP observations for the three latitude bands

have been additionally separated into day-time (12:00–15:00 Local Time LT) and night-time (00:00–03:00 LT) intervals.

2.2.3 MOPITT CO total column retrievals

The MOPITT (Measurement Of Pollution In The Troposphere) instrument is mounted on board the NASA EOS Terra satellite and provides CO distributions at the global scale (Deeter et al., 2004). MOPITT has a horizontal resolution of 22 km x 22 km and allows global coverage within 3 days. The data used in this study corresponds to CO total columns from version 5 (V5) of the MOPITT thermal infrared (TIR) product level 3. This product is available via the following web server: <http://www2.acd.ucar.edu/mopitt/products>. Validation of the MOPITT V5 product against in-situ CO observations showed a mean bias of 0.06×10^{18} molecules cm^{-2} (Deeter et al., 2013). Following the recommendation in the users' guide, (www.acd.ucar.edu/mopitt/v5_users_guide_beta.pdf), the MOPITT data were averaged by taking into account their relative errors provided by the Observation Quality Index (OQI).

Also, in order to achieve better data quality we used only daytime CO data since retrieval sensitivity is greater for daytime rather than nighttime overpasses. A further description of the V5 data is presented in Deeter et al. (2013) and Worden et al. (2014).

For the validation, the model CO profiles (X) were transformed by applying the MOPITT averaging kernels (A) and the a priori CO profile (X_a) according to the following equation (Rodgers, 2000) to derive the smoothed profiles X^* appropriate for comparison with MOPITT data:

$$X^* = X_a + A(X - X_a)$$

Details on the method of calculation are referred to in Deeter et al. (2004) and Rodgers (2000). The averaging kernels indicate the sensitivity of the MOPITT measurement and retrieval system to the true CO profile, with the remainder of the information set by the a priori profile and retrieval constraints (Emmons, 2009; Deeter et al., 2010). The CO data X^* (derived using the above equation) have the same vertical resolution and a priori dependence as the MOPITT retrievals and have been used to calculate averaging kernel smoothed model CO total columns, which are compared to the MOPITT CO total columns. For the evaluation, 8 regions are defined (see Fig. 1): Europe, Alaska, Siberia, North Africa, South Africa, South Asia, East Asia and the United States.

The model update in July 2012 includes an integration of MOPITT CO total columns in the model's data assimilation system. With this, the MOPITT validation data has lost its independency for the rest of the validation period and MOPITT validation data has thus only been used until June 2012 for validation purposes.

2.2.4 SCIAMACHY and GOME-2 NO₂ satellite observations

The SCanning Imaging Absorption spectroMeter for Atmospheric CHartography (SCIAMACHY; Bovensmann et al., 1999) onboard the ENVISAT and the Global Ozone Monitoring Experiment-2 (GOME-2; Callies et al., 2000) onboard the Meteorological Operational Satellite-A (MetOp-A) comprise UV-VIS and NIR sensors designed to provide global observations of atmospheric trace gases.

In this study, the tropospheric NO₂ column data set described in Hilboll et al. (2013a) has been used. In short, the measured radiances are analysed using Differential Optical Absorption Spectroscopy (DOAS), (Platt and Stutz, 2008) in the 425–450 nm wavelength window (Richter and Burrows, 2002). The influence of stratospheric NO₂ air masses has been accounted for using the algorithm detailed by Hilboll et al. (2013b), using stratospheric NO₂ fields from the Bremen 3D Chemistry and Transport Model (B3dCTM, see also Sinnhuber et al., 2003a; Sinnhuber et al., 2003b; Winkler et al., 2008). Tropospheric air mass factors have been calculated with the radiative transfer model SCIATRAN (Rozanov et al., 2005). Only measurements with Fast RETrieval Scheme for Cloud from Oxygen A band (FRESCO+) algorithm (Wang et al., 2008) cloud fractions of less than 20% are used.

Tropospheric NO₂ vertical column density (VCD) from the MACC_osuite is compared to tropospheric NO₂ VCD from GOME-2 and SCIAMACHY. As the European Space Agency lost contact with ENVISAT in April 2012, GOME-2 data is used for model validation from 1 April 2012 onwards, while SCIAMACHY data is used for the remaining time period (September 2009 to March 2012). Satellite observations are gridded to the horizontal model resolution, i.e. 1.875° for IFS cycle CY36R1 (09/2009 -06/2012) and 1.125° for cycle CY37R3 (07/2012- 12/2012).

A few processing steps are applied to the MACC_osuite data to account for differences to the satellite data such as observation time. Firstly, model data are vertically integrated to tropospheric NO₂ VCDs by applying National Centers for Environmental Prediction (NCEP) reanalysis (Kalnay et al., 1996) climatological tropopause pressure shown in Fig.1 of Santer et

al. (2003). Secondly, simulations are interpolated linearly in time to the SCIAMACHY equator crossing time (roughly 10:00 LT). This most likely leads to some minor overestimation of model NO₂ VCDs compared to GOME-2 data, as the equator crossing time for GOME-2 is about 9:30 LT. Moreover, only model data for which corresponding satellite observations exist are considered. For the evaluation, the same regions have been used as for MOPITT (Fig.1), except for Siberia and Alaska. In contrast to MOPITT data, no averaging kernel is applied.

Satellite observations of tropospheric NO₂ columns have relatively large uncertainties, mainly linked to incomplete stratospheric correction (important over clean regions and at high latitudes in winter and spring) and to uncertainties in air mass factors (mainly over polluted regions) (e.g. Boersma et al., 2004 and Richter et al., 2005). The uncertainty varies with geolocation and time but in first approximation can be separated into an absolute error of 5×10^{14} molec cm⁻² and a relative error of about 30%, whichever is larger. As some of the contributions to this uncertainty are systematic, averaging over longer time periods does not reduce the errors as much as one would expect for random errors. Over polluted regions, the uncertainty from random noise in the spectra is small in comparison to other error sources, in particular for monthly averages.

2.3 Validation metrics

A comprehensive model evaluation requires the selection of validation metrics that provide complementary aspects of model performance. The following metrics have been used in the evaluation:

Modified Normalized Mean Bias MNMB

$$MNMB = \frac{2}{N} \sum_i \frac{f_i - o_i}{f_i + o_i} \quad (1)$$

Root Mean Square Error RMSE

$$RMSE = \sqrt{\frac{1}{N} \sum_i (f_i - o_i)^2} \quad (2)$$

Correlation Coefficient

$$R = \frac{\frac{1}{N} \sum_i (f_i - \bar{f})(o_i - \bar{o})}{\sigma_f \sigma_o} \quad (3)$$

where: N is the number of observations, f are the modelled analysis and o the observed values, \bar{f} and \bar{o} are the mean values of the analysis and observed values and σ_f and σ_o are the corresponding standard deviations.

The validation metrics above have been chosen to provide complementary aspects of model performance. The modified normalized mean bias is a normalization based on the mean of the observed and forecast value (e.g. Elguindi et al. 2010). It ranges between -2 and 2 and when multiplied by 100%, it can be interpreted as a percentage bias.

We chose to use the MNMB in our evaluations because verifying chemical species concentration values significantly differs from verifying standard meteorological fields. For example, spatial or temporal variations can be much greater and the differences between model and observed values (“model errors”) are frequently much larger in magnitude. Most importantly, typical concentrations can vary quite widely between different pollutant types (e.g. O_3 and CO) and region (e.g. Europe vs. Antarctica), and a given bias or error value can have a quite different significance. It is useful therefore to consider bias and error metrics which are normalized with respect to observed concentrations and hence can provide a consistent scale regardless of pollutant type (see e.g. Elguindi et al., 2010 or Savage et al., 2013). Moreover, the MNMB is robust to outliers and converges to the normal bias for biases approaching zero, while taking into account the representativeness issue when comparing coarse resolved global models versus site specific station observations. Though GAW stations prove regionally representative in general, the experience is that local effects cannot always be ruled out reliably in long worldwide data sets, because transport, chemical processes and parameterizations are not selective for the super- to sub-grid-scale threshold. Referencing to the model/observation mean again constitutes a pragmatic workaround to avoid misleading bias tendencies, particularly in sensitive regions with sparse data coverage. Within MACC, the MNMB is used as an important standard score. It is used in the MACC quarterly evaluation reports and it appears in a lot of recent publications, e.g. Cuevas et al. (2015), Eskes et al. (2015), Sheel et al. (2014).

The MNMB varies symmetrically with respect to under- and overestimation. However, when calculated over longer time periods, a balance in model error, with model over-and

underestimation compensating each other, can lead to a small MNMB for the overall period. For this reason, it is important to additionally consider an absolute measure, such as the RMSE. However, it has to be noted that the RMSE is strongly influenced by larger values and outliers, due to squaring. The correlation coefficient R can vary between 1 (perfect correlation) and -1 (negative correlation) and is an important measure to check the linearity between model and observations.

3 Results

3.1 Evaluation of ozone

The evaluation of the MACC_osuite run with O_3 from GAW surface observations (described in section 2.2.1) demonstrates good agreement in absolute values and seasonality for most regions. Figure 2 shows maps with Modified Normalized Mean Bias (MNMB, see section 2.3) evaluations for 50 GAW stations globally (top) and in Europe (bottom). Figure 3 presents selected time series plots representing the results for high latitudes, low latitudes and Europe. Large negative MNMBs over the whole period 09/2009 to 12/2012 (-30 to -82%) are observed for stations located in Antarctica (Neumayer-NEU, South Pole-SPO, Syowa-SYO and Concordia- CON) whereby O_3 surface mixing ratios are strongly underestimated by the model. For stations located in high latitudes in the northern hemisphere (Barrow-BAR, Alaska and Summit-SUM, Denmark), the MACC_osuite exhibits similar underestimated values of up to -35% for the whole evaluation period. The time series plots for Arctic and Antarctic stations (e.g. Summit-SUM, Neumayer-NEU and South Pole-SPO) in Fig. 3 show that an underestimation visible in these regions appears to be remedied and model performance improved with an updated dry deposition parameterization over ice, which has been introduced with the new model cycle in July 2012 (see section 2.1).

Large positive MNMBs (up to 50 to 70%, Fig. 2) are observed for stations that are located in or nearby cities and thus exposed to regional sources of contamination (Iskrba-ISK Slovenia, Tsukuba- TSU, Japan, Cairo-CAI, Egypt). In tropical and subtropical regions, O_3 surface mixing ratios are systematically overestimated (by about 20% on average) during the evaluation period. The time series plots for tropical and subtropical stations (e.g. for Ragged Point-RAG, Barbados and Cape Verde Observatory, Cape Verde –CVO, Fig. 3) reveal a slight systematic positive offset throughout the year, however with high correlation coefficients (0.6 on average).

For GAW stations in Europe, the evaluation of the MACC_osuite for the whole period shows MNMBs between -80 and 67%. Large biases appear only for 2 GAW stations located in Europe: Rigi- RIG, Switzerland (-80%), located near mountainous terrain and Iskrba- ISK, Slovenia (67%). For the rest of the stations MNMBs lie between 22 and -30%. Root Mean Square Errors (RMSEs, see section 2.3) range between 7 and 35 ppb (15 ppb on average). Again, results for Iskrba-ISK and Rigi-RIG show the largest errors. All other stations show RMSEs between 7 and 20 ppb. Correlation coefficients here range between 0.1 and 0.7 (with 0.5 on average). Table 4 summarizes the results for all stations individually.

Monthly MNMBs (see Fig. 4) show a seasonally varying bias, with positive MNMBs occurring during the northern summer months (with global average ranging between 5 and 29% during the months June and October), and negative MNMBs during the northern winter months (between -2 and -33% during the months December to March). These deviations partly cancel each other out in MNMB for the whole evaluation period. For the RMSEs, (Fig. 5) maximum values also occur during the northern summer months with global average ranging between 11 and 16 ppb for June to September. The smallest errors appear during the northern hemisphere winter months (global average falling between 8 and 10 ppb for December and January). The correlation does not show a distinct seasonal behaviour (see Fig. 6).

The time series plots in Fig. 3 show that the seasonal cycle of O₃ mixing ratios with maximum concentrations during the summer months and minimum values occurring during winter times for European stations (e.g. Monte Cimone-MCI, Italy, Kosetice-KOS, Czech Republic, and Kovk- KOV, Slovenia), could well be reproduced by the model, although there is some overestimation in summer resulting mostly from observed minimum concentrations that are not captured correctly by the MACC_osuite, (Kosetice-KOS, Czech Republic, and Kovk- KOV, Slovenia).

The validation with EMEP surface ozone observations (described in section 2.2.2) in three different regions in Europe for the period 09/2009 to 12/2012 likewise confirms the behaviour of the model to overestimate O₃ mixing ratios during the warm period and underestimate O₃ concentrations during the cold period of the year (see Fig. 7). The mostly positive bias (May-November) is between -9 and 56% for northern Europe and Central Europe and between 8% and 48% for Southern Europe. Negative MNMBs appear, in accordance with GAW validation results, during the winter-spring period (December-April) ranging between -48 and -7% for

EMEP stations in northern Europe (exception: December 2012 with 25%), between -1 and -39% in central Europe (exception: December 2012 with 31%), whereas in southern Europe, deviations are smaller and remain mostly positive (between -8 and 9%) in winter (exception: December 2012 with 37%). The different behaviour for December 2012 likely results from the limited availability of observations towards the end of the validation period. The separate evaluation of day and night-time O₃ mixing ratios (Fig. 8) shows that for northern Europe night time biases exceed day time biases during all seasons. For central Europe and southern Europe night-time biases are larger (negative MNMBs) during cold periods (December-April), whereas during warm periods (May–November) larger biases (positive MNMBs) appear during day time.

3.2 Evaluation of carbon monoxide

The evaluation of the MACC_osuite with surface observations of 29 GAW stations (described in section 2.2.1) shows that over the whole period September 2009 to December 2012, CO mixing ratios could be reproduced with an average MNMB of -10%. The MNMBs for all stations range between -50 and +30%. Results are listed in Table 5, a selection of time series plots shows the results for stations in Europe, Asia and Canada in Fig. 9. MNMBs exceeding $\pm 30\%$ appear for stations that are either located in or nearby cities and thus exposed to regional sources of contamination (Kosetice- KOS, Czech Republic) or are located in or near complex mountainous terrain (Rigi-RIG, Switzerland, BEO Moussala- BEO, Bulgaria) which is not resolved by the topography of the global model. RMSEs fall between 12 and 143 ppb (on average 48 ppb) for all stations during the validation period, but for only four stations (Rigi-RIG, Kosetice- KOS, Payerne-PAY, Switzerland and BEO Moussala-BEO, all located in Europe) do the RMSEs exceed 70 ppb. Correlation coefficients from the comparison with GAW station data calculated over the whole time period range between 0 and 0.8 (on average 0.4), with only four stations showing values smaller than 0.2 (Rigi-RIG, Moussala-BEO, East Trout Lake-ETL and Lac la Biche-LAC (the latter two located in Canada).

Considering the global monthly MNMBs and RMSEs, it can be seen that during the northern hemisphere summer months, June to September, both are small (absolute differences less than 5%), see Fig. 10 and Fig. 11. Negative MNMBs (up to -35%) and larger RMSEs (up to 72 ppb) appear during the northern hemisphere winter months, November to March, when anthropogenic emissions are at a highest, especially for the US, northern latitudes and Europe. Monthly correlation coefficients are between 0.1 and 0.5 and do not show a distinct seasonal

behaviour (see Fig. 12), the low values of 0.1 during the period January 2011 to October 2011 result from the reading error in the fire emissions (see section 2.1.1). The generally only moderate correlation coefficient is related to mismatches in the strong short-term variability seen in both the model and the measurements.

The time series plots for stations in Europe, Asia and Canada in Fig. 9 demonstrate that the annual CO cycle could to a large degree be reproduced correctly by the model with maximum values occurring during the winter period and minimum values appearing during the summer season. However, the model shows a negative offset during the winter period. Seasonal air mass transport patterns that lead to regular annual re-occurring CO variations could be reproduced for GAW stations in East Asia: The time series plots for Yonagunijima- YON and Minamitorishima- MNM station, Japan (Fig. 9) show that the drop of CO, associated with the air mass change from continental to cleaner marine air masses after the onset of the monsoon season during the early summer months, is captured by the MACC_osuite. Deterioration in all scores is visible during December 2010 in the time series plots of several stations (e.g. Jungfraujoch-JFJ, and Sonnblick-SBL, Fig. 9). This is likely a result of changes in the processing of the L2 IASI data and a temporary blacklisting of IASI data (to avoid model failure) in the assimilation.

The comparison with MOPITT satellite CO total columns between October 2009 and June 2012 (described in section 2.2.3) shows a good qualitative agreement of spatial patterns and seasonality, see Table 6. The MNMBs for 8 regions are listed in Fig. 13 and range between -22% and 14%. The seasonality of the satellite observations is captured well by the MACC_osuite over Asia and Africa, with MNMBs between -6% and 9% (North Africa), -12% and 8% (South Africa), -11% and 12% (East Asia), and -3% and 14% (South Asia). The largest negative MNMBs appear during the winter periods, especially from December 2010 to May 2011 and from September 2011 to April 2012, for Alaska and Siberia and for the US and Europe (MNMBs up to -22%), which coincides with large differences between MOPITT and IASI satellite data (see Fig. 14). On the global scale the average difference between the IASI and MOPITT total columns is less than 10% (George et al., 2009), and there is a close agreement of MOPITT and IASI for S. Asia and Africa (see Fig. 14). However, larger differences between MOPITT and IASI data appear during the northern winter months over Alaska, Siberia, Europe and the US, which result in lower CO concentrations in the model, due to the assimilation of IASI CO data in the MACC_osuite. The differences between

MOPITT and IASI data can be mainly explained by the use of different a priori assumptions in the IASI and MOPITT retrieval algorithms (George et al., 2015). Indeed, the Fast Optimal Retrievals on Layers for IASI (FORLI) software (IASI) is using a single a priori CO profile (with an associated variance-covariance matrix) whereas the MOPITT retrieval algorithm is using a variable a priori, depending on time and location. George et al., (2015) show that differences above Europe and the US in January and December (for a 5 year study) decrease by a factor of 2 when comparing IASI with a modified MOPITT product using the IASI single a priori. Between January 2011 and October 2011 there has also been a reading error in the fire emissions that contributes to larger MNMBs during this period (see section 2.1.1).

3.3 Evaluation of tropospheric nitrogen dioxide

Figure 15 shows global maps of daily tropospheric NO₂ VCD averaged from September 2009 to March 2012. Overall, spatial distribution and magnitude of tropospheric NO₂ observed by SCIAMACHY are well reproduced by the model. This indicates that emission patterns and NO_x photochemistry are reasonably well represented by the model. However, the model underestimates tropospheric NO₂ VCDs over industrial areas in Europe, East China, Russia, and South East Africa compared to satellite data. This could imply that anthropogenic emissions from RETRO-REAS are too low in these regions, or that the lifetime in the model is too short. The model simulates larger NO₂ VCD maxima over Central Africa, which mainly originate from wild fires. It remains unclear if GFEDv2/GFAS fire emissions are too high here or if NO₂ fire plumes closer to the ground cannot be seen by the satellites due to light scattering by biomass burning aerosols (Leitao et al., 2010). In the northern hemisphere, background values of NO₂ VCD over the ocean are lower in the simulations than in the satellite data. The same is true for the South Atlantic Ocean to the west of Africa (see Fig.15). This might suggest a model underestimation of NO₂ export from continental sources or too rapid conversion of NO₂ into its reservoirs. However, as the NO₂ columns over the oceans are close to the uncertainties in the satellite data, care needs to be taken when interpreting these differences.

Time series of daily tropospheric NO₂ VCD averaged over different regions and corresponding monthly means are presented in Figs. 16 and 17, respectively. Time series of the MNMB and RMSE are shown in Figs. 18 and 19, respectively. Table 7 summarizes the statistical values derived over the whole time period. High anthropogenic emissions occur over the United States, Europe, South Asia and East Asia compared to other regions on the

globe (e.g., Richter et al., 2005). In principle, the MACC_osuite catches the pattern of satellite NO₂ VCD over these regions. However, the model tends to underestimate NO₂ VCDs throughout the whole time period investigated here. The negative bias is most pronounced over East Asia with a modelled mean NO₂ VCD for September 2009 to December 2012 of about 3.8×10^{15} molec cm⁻² lower than that derived from satellite measurements (see Table 7).

Considering monthly values, the MACC_osuite strongly underestimates magnitude and seasonal variation of satellite NO₂ VCD over East Asia (MNMBs between about -40 % and -110 % and RMSE between 1×10^{15} molec cm⁻² and 14×10^{15} molec cm⁻² throughout the whole time period). A change in the modelled NO₂ values is apparent in July 2012 when the emission inventories changed and the agreement with the satellite data improved for South and East Asia but deteriorated for the US and Europe. This results in a drop of MNMBs (Fig. 18) for Europe and the US with values approaching around -70% by the end of 2012. Nevertheless, correlations between daily satellite and model data derived for the whole time period (see Table 7) are high for East Asia (0.8), South Asia (0.8), Europe (0.8), and lower, but still rather high, for the US (0.6).

The North African and South African regions are strongly affected by biomass burning (Schreier et al., 2013). Magnitude and seasonality of daily and monthly tropospheric NO₂ VCDs (Figs. 16 and 17, respectively) are rather well represented by the model, apart from January 2011 to October 2011, due to difficulties in reading fire emissions for this time period (see section 2.1.1). The latter results in large absolute values of the MNMB (Fig. 18) and large RMSEs (Fig. 19) between January 2011 and October 2011 compared to the rest of the time period. As for other regions investigated in this section, mean values of simulated daily tropospheric NO₂ VCDs over North Africa and South Africa between September 2009 and December 2012 tend to be lower than the corresponding satellite mean values (see Table 7). The correlation between daily model and satellite data over the whole time period is about 0.6 for South Africa and 0.5 for North Africa. It should be investigated in future studies, if this difference in model performance for the African regions is due to meteorology, chemistry or emissions.

The evaluation of modelled NO₂ with GAW surface data for 6 European stations accordingly shows that NO₂ is generally underestimated at the surface. MNMBs are typically in the range of -26% and -45%, larger MNMBs appear only for two stations in complex mountainous

terrain (Rigi-RIG 68% and Sonnblick-SBL -160%). RMSEs are between 0.3 and 9 ppb, correlation coefficients between 0.1 and 0.6 for the period between 9/2009 and 12/ 2012, see Table 8. The annual cycle of NO₂ with maximum concentrations during the winter period is in principle captured by the model, shown in the time series plots in Fig. 20. As is observed for the satellite VCDs, NO₂ surface concentrations decrease in the model with the introduction of the updated model version and emission inventories. For stations located in complex terrain (e.g. Rigi, Fig. 20), results improve after the model update, likely also due to the higher model resolution. Monthly values of MNMB, R and correlation coefficient are shown in Figs. 21 to 23.

4 Discussion

The validation of global O₃ mixing ratios with GAW observations at the surface levels showed that the MACC_osuite could generally reproduce the observed annual cycle of ozone mixing ratios. Model evaluation with surface data shows global average monthly MNMBs between -30% and 30% (GAW) and for Europe between -50% and 60% (EMEP). For stations located in the northern mid-latitudes, the evaluation reveals a seasonally dependent bias, with an underestimation of the observed O₃ mixing ratios by the MACC_osuite during the winter season and an overestimation during the summer months. The validation of day-time versus night-time concentrations for Northern and Central Europe shows larger negative MNMBs in the winter months during night time than day time (Fig. 8), so that the negative bias in winter could be attributed to the simulation of vertical mixing at night, also described by Ordoñez (2010) and Schaap (2008), which remains a challenge in the model. The systematic underestimation of O₃ mixing ratios throughout the year for high latitude northern regions and Antarctica has its origin in an overestimation of the O₃ dry deposition velocities over ice. With the implementation of the new model cycle and the updated MOZART model version, which includes updated velocity fields for the dry deposition of O₃, as described in Stein et al. (2013), the negative offset in the MACC_osuite model has been remedied for high latitude regions from July 2012 onwards (see the time series plots for the South Pole station- SPO and Neumayer- NEU in Fig. 3). The overestimation of O₃ mixing ratios during the summer months is a well-known issue and has been described by various model validation studies (e.g., Brunner et al., 2003, Schaap et al., 2008, Ordoñez et al., 2010, Val Martin et al., 2014). Inadequate ozone precursor concentrations and aerosol induced radiative effects (photolysis)

1 have been frequently identified as being the main factors. The time series plots in Fig. 3,
2 however, demonstrate that the minimum concentrations in particular are not captured by the
3 model during summer. Possible explanations include a general underestimation of NO
4 titration which especially applies to stations with urban surroundings and strong sub-grid
5 scale emissions (e.g. Tsukuba-TSU Fig. 3), including difficulties by the global model to
6 resolve NO titration in urban plumes. It also seems likely that dry deposition at wet surfaces
7 in combination with the large surface sink gradient due to nocturnal stability cannot be
8 resolved with the model's vertical resolution. In regions such as Central and Southern Europe
9 (Fig. 8) where day time biases exceed night time biases, the overestimation of O₃ might be
10 related to an underestimation of day-time dry deposition velocities: Val Martin et al., (2014)
11 describe a reduction of the summertime O₃ model bias for surface ozone after the
12 implementation of adjustments in stomatal resistances in the MOZART model's dry
13 deposition parameterization.

14 The MACC_osuite model realistically reproduces CO total columns over most of the
15 evaluated regions with monthly MNMBs falling between 10% and -20% (Table 6). There is
16 close agreement of modelled CO total columns and satellite observations for Africa and South
17 Asia throughout the evaluation period. However, there is a negative offset compared to the
18 observational CO data over Europe and North America. The largest deviations occur during
19 the winter season when the observed CO concentrations are highest. The evaluation with
20 GAW surface CO data accordingly shows a wintertime negative bias of up to -35% at the
21 surface for stations in Europe and the US. A general underestimation of CO from global
22 models in the northern hemisphere has been described by various authors (e.g., Shindell et al.,
23 2006, Naik et al., 2013). According to Stein et al. (2014) this underestimation likely results
24 from a combination of errors in the dry deposition parameterization and certain limitations in
25 the current emission inventories. The latter include too low anthropogenic CO emissions from
26 traffic or other combustion processes and missing anthropogenic VOC emissions in the
27 inventories together with an insufficiently established seasonality in the emissions. An
28 additional reason for the apparent underestimation of emissions in MACCcity may be an
29 exaggerated downward trend in the RCP8.5 (Representative Concentration Pathways)
30 scenario in North America and Europe between 2000 and 2010, as this scenario was used to
31 extrapolate the MACCcity emissions from their bench mark year, i.e. 2000. For CO,
32 uncertainties in the evaluation also include the retrieved amount of CO total columns between
33 IASI and MOPITT. These vary with region, with IASI showing lower CO concentrations in

several regions (Alaska, Siberia, Europe and the US) during the northern winter months, which possibly contribute to the deviations observed between the modelled data and MOPITT satellite data, as only IASI data has been assimilated in the model. The differences can primarily be explained by the use of different a priori assumptions in the IASI and MOPITT retrieval algorithms (George et al., 2015). On a global scale however, the average difference between the IASI and MOPITT total columns is less than 10% (George et al., 2009). From July 2012 onwards, MOPITT CO total columns are also assimilated in the MACC_osuite.

Modelled NO₂ tropospheric columns agree well with satellite observations over the United States, South Asia and North Africa. However, there is also a negative offset for NO₂ over East Asia and Europe. For the latter, these findings are supported by the evaluation with GAW surface data. Again, the largest deviations are occurring during the winter season. The quality of the emission inventory is even more crucial for short lived reactive species such as NO₂, where model results depend to a large extent on emission inventories incorporated in the simulations. This is highlighted by the deterioration of agreement between model results and satellite data for the US in July 2012 when anthropogenic emissions were changed from RETRO-REAS to MACCCity. This change led to an increasing negative bias in NO₂ over Europe and North America and to an improvement for South and East Asia (see Fig. 18). A deterioration in MNMBs associated with the fire emissions is visible between January 2011 and October 2011 over regions with heavy fire activity (Africa and East Asia), and goes back to a temporary error in the model regarding the reading of fire emissions (see Figs. 17 and 18). Particular challenges for an operational forecast system are regions with rapid changes in emissions such as China, where inventories need to be extrapolated to obtain reasonable trends. A large underestimation of NO₂ in China especially in winter has been reported for other CTMs in previous publications (He et al., 2007, Itahashi et al., 2014). The latter has been linked to an underestimation of NO_x and VOC emissions, unresolved seasonality in the emissions and expected non-linearity of NO_x chemistry. The change in validation data sets from SCIAMACHY to GOME-2 has shown to have negligible impact on the validation results and conclusions.

5 Conclusion

The MACC_osuite is the global near-real-time MACC model analysis run for aerosol and reactive gases. The model has been evaluated with surface observations and satellite data

concerning its ability to simulate reactive gases in the troposphere. Results showed that the model proved capable of a realistic reproduction of the observed annual cycle for CO, NO₂ and O₃ mixing ratios at the surface, however, with seasonally dependent biases. For ozone, these seasonal biases likely result from difficulties in the simulation of vertical mixing at night and deficiencies in the model's dry deposition parameterization. For CO, a negative offset in the model during the winter season is attributed to limitations in the emission inventories together with an insufficiently established seasonality in the emissions.

NO₂ total columns derived from satellite sensors and surface NO₂ observed by European GAW stations could be reproduced reasonably well over most of the evaluated regions, but showed a negative offset compared to the observational data, especially over Europe and East Asia (NO₂). It has become clear, that the emission inventories play a crucial role for the quality of model results and remain a challenge for near-real-time modeling, especially over regions with rapid changes in emissions. Inconsistencies in the assimilated satellite data and fire emissions showed only a temporary impact on the quality of model results. The implementation of a model update improved the results especially in the high latitudes (surface ozone) and over South and East Asia (NO₂).

The MACC NRT forecast system is constantly evolving. A promising step in model development is the on-line integration of modules for atmospheric chemistry in the IFS, currently being tested for implementation in the MACC_osuite. In contrast to the coupled model configuration as used in this paper, the on-line integration in the Composition IFS (C-IFS) provides major advantages; apart from an enhanced computational efficiency, C-IFS promises an optimization of the implementation of feedback processes between gas-phase/aerosol chemical processes and atmospheric composition and meteorology, which is expected to improve the modeling results for reactive gases. Additionally, C-IFS will be available in combination with different CTMs, (MOZART and TM5), which will help to explain whether deviations between model and observations go back to deficiencies in the chemistry scheme of a model.

Acknowledgements

This work has been carried out in the framework of the MACC projects, funded under the EU Seventh Research Framework Programme for research and technological development. The authors thank the MACC validation and reactive gas subproject teams for the fruitful discussions. Model simulations were carried out using the ECMWF supercomputer. We wish

to acknowledge the provision of GAW hourly station data from the World Data Centre of Greenhouse Gases (WDCGG) and hourly EMEP station data from the NILU database. Specifically, we like to thank: the CSIRO Oceans and Atmosphere Flagship for making the data freely available and the Australian Bureau of Meteorology for continued operation and support of the Cape Grim station. We also like to thank Izaña Atmospheric Research Center (AEMET) for providing CO and O₃ data. Special thanks to the providers of NRT data to the MACC project, namely: Institute of Atmospheric Sciences and Climate (ISAC) of the Italian National Research Council (CNR), South African Weather Service, The University of York and National Centre for Atmospheric Science (NCAS (AMF)) (UK), and the Instituto Nacional de Meteorologia e Geofisica (INMG) (Cape Verde), National Air Pollution Monitoring Network (NABEL) (Federal Office for the Environment FOEN and Swiss Federal Laboratories for Materials Testing and Research EMPA), Japan Meteorological Agency (JMA), Alfred Wegener Institute, Umweltbundesamt (Austria), National Meteorological Service (Argentina), Umweltbundesamt (UBA, Germany). We thank the National Center for Atmospheric Research (NCAR) MOPITT science team and the NASA Langley Research Center, Atmospheric Science Data Center (ASDC), for producing and archiving the MOPITT CO product. IASI has been developed and built under the responsibility of the Centre National D'Etudes Spatiales (CNES, France). We are grateful to Juliette Hadji-Lazaro and the UBL/ LATMOS IASI team for establishing the IASI-MACC near real time processing chain. We wish to acknowledge that SCIAMACHY lv1 (level 1) radiances were provided to the Institute of Environmental Physics, University of Bremen by ESA through DLR/DFD.

References

- Aas, W., Hjellbrekke, A.-G., Schaug, J.: Data quality 1998, quality assurance and field comparisons. Kjeller, Norwegian Institute for Air Research (EMEP/CCC-Report 6/2000), 2000.
- Ashmore, M. R.: Assessing the future global impacts of ozone on vegetation. *Plant Cell Environ.* 28, 949–964, 2005.
- Ballabrera-Poy, J., Kalnay, E. and Yang, S.: Data assimilation in a system with two scales—combining two initialization techniques. *Tellus* (2009), 61A, 539–549, doi:10.1111/j.1600-0870.2009.00400.x, 2009.
- Bell M.L., R.D. Peng and F. Dominici: The exposure–response curve for O₃ and risk of mortality and the adequacy of current O₃ regulations. *Environmental Health Perspectives*,

1 114 (4), 2006.

2 Benedetti, A., Morcrette, J.-J., Boucher, O., Dethof, A., Engelen, R. J., Fisher, M., Flentje, H.,
3 Huneus, N., Jones, L., Kaiser, J. W., Kinne, S., Mangold, A., Razinger, M., Simmons, A. J.,
4 Suttie, M., and the GEMS-AER team: Aerosol analysis and forecast in the European Centre
5 for Medium-Range Weather Forecasts Integrated Forecast System: Data Assimilation. *J.*
6 *Geophys. Res.*, D13205, 114, doi:10.1029/2008JD011115, 2008.

7 Benedetti, A., Kaiser, J. W., and Morcrette J.-J.: [Global Climate] Aerosols [in "State of the
8 Climate in 2010"]. *B. Am.Meterol. Sci.*, 92(6):S65–S67, 2011.

9 Boersma, K.F., Eskes, H.J., Brinksma, E.J.: Error analysis for tropospheric NO₂ retrieval
10 from space. *J. Geophys. Res.*, 109, D4, doi:10.1029/2003JD003962, 2004.

11 Bovensmann, H., J. P. Burrows, M. Buchwitz, J. Frerick, S. Noël, V. V. Rozanov, K. V.
12 Chance, A. P. H. Goede: SCIAMACHY: Mission Objectives and Measurement Modes. *J.*
13 *Atmos. Sci.*, 56, 127–150, 1999.

14 Brunner, D., Staehelin, J., Rogers, H. L., Köhler, M. O., Pyle, J. A., Hauglustaine, D.,
15 Jourdain, L., Berntsen T. K., Gauss, M., Isaksen, I. S. A., Meijer, E., van Velthoven, P.,
16 Pitari, G., Mancini, E., Grewe, V. and Sausen, R.: An evaluation of the performance of
17 chemistry transport models by comparison with research aircraft observations. Part 1:
18 Concepts and overall model performance. *Atmos. Chem. Phys.*, 3, 1609–1631,
19 doi:10.5194/acp-3-1609-2003, 2003.

20 Callies, J., Corpaccioli, E., Eisinger, M., Hahne, A., and Lefebvre, A.: GOME-2 Metop's
21 Second-Generation Sensor for Operational Ozone Monitoring, *ESA Bull.*, 102, 28–36, 2000.

22 Cammas, J.-P., A. Gilles, S. Chabrillat, F. Daerden, N. Elguindi, J. Flemming, H. Flentje, C.
23 Deshler, T., J.L. Mercer, H.G.J. Smit, R. Stubi, G. Levrat, B.J. Johnson, S.J. Oltmans, R.
24 Kivi, A.M. Thompson, J. Witte, J. Davies, F.J. Schmidlin, G. Brothers, T. Sasaki
25 Atmospheric comparison of electrochemical cell ozonesondes from different manufacturers,
26 and with different cathode solution strengths: The Balloon Experiment on Standards for
27 Ozonsondes. *J. Geophys. Res.* 113, D04307, doi:10.1029/2007JD008975, 2008.

28 Cape, J.N.: Surface ozone concentrations and ecosystem health: Past trends and a guide to
29 future projections. *Science of the Total Environment* Vol. 400, 257-269.,
30 doi:10.1016/j.scitotenv.2008.06.025, 2008.

Clarisse, L., R'Honi, Y., Coheur, P.-F., Hurtmans, D., and Clerbaux, C.: Thermal infrared nadir observations of 24 atmospheric gases, *Geophys. Res. Lett.*, 38, L10802, doi:10.1029/2011GL047271, 2011.

Clerbaux, C., Boynard, A., Clarisse, L., George, M., Hadji-Lazaro, J., Herbin, H., Hurtmans, D., Pommier, M., Razavi, A., Turquety, S., Wespes, C., and Coheur, P.-F.: Monitoring of atmospheric composition using the thermal infrared IASI/MetOp sounder, *Atmos. Chem. Phys.*, 9, 6041–6054, doi:10.5194/acp-9-6041-2009, 2009.

Cooper, O. R., Parrish, D. D., Ziemke, J., Balashov, N. V., Cupeiro, M., Galbally, I. E., Gilge, S., Horowitz, L., Jensen, N. R., Lamarque, J.-F., Naik, V., Oltmans, S. J., Schwab, J., Shindell, D. T., Thompson, A. M., Thouret, V., Wang, Y., Zbinden, R. M.: Global distribution and trends of tropospheric ozone: an observation-based review, *Elem. Sci. Anth.*, 2, 10 000029, doi:10.12952/journal.elementa.000029, 2014.

Cuevas, E., Camino, C., Benedetti, A., Basart, S., Terradellas, E., Baldasano, J.M., Morcrette, J.-J., Marticorena, B., Goloub, P., Mortier, A., Berjón, A., Hernández, Y., Gil-Ojeda, M., Schulz, M.: The MACC-II 2007-2008 Reanalysis: Atmospheric Dust Evaluation and Characterization over Northern Africa and Middle East, *Atmos. Chem. Phys.* 15, 3991–4024, doi:10.5194/acp-15-3991-2015, 2015.

Deeter, M. N., Emmons, L. K., Edwards, D. P., Gille, J. C., and Drummond, J. R.: Vertical resolution and information content of CO profiles retrieved by MOPITT, *Geophys. Res. Lett.*, 31, L15112, doi:10.1029/2004GL020235, 2004.

Deeter, M. N., et al.: The MOPITT version 4 CO product: Algorithm enhancements, validation, and long-term stability, *J. Geophys. Res.*, 115, D07306, doi:10.1029/2009JD013005, 2010.

Deeter, M. N., H. M. Worden, D. P. Edwards, J. C. Gille, D. Mao, and J. R. Drummond: MOPITT multispectral CO retrievals: Origins and effects of geophysical radiance errors, *J. Geophys. Res.*, 116, doi:10.1029/2011JD015703, 2011.

Deeter, M. N., Worden, H. M., Edwards, D. P., Gille, J. C., Andrews, A. E.: evaluation of MOPITT retrievals of lower-tropospheric carbon monoxide over the United States, *J. Geophys. Res.*, 117, D13306, doi:10.1029/2012JD017553, 2012.

Deeter, M. N., Martínez-Alonso, S., Edwards, D. P., Emmons, L. K., Gille, J. C., Worden, H. M., Pittman, J. V., Daube, B. C., Wofsy, S. C.: Validation of MOPITT Version 5 thermal-

1 infrared, near-infrared, and multispectral carbon monoxide profile retrievals for 2000–2011, J.
2 Geophys. Res. Atmos., 118, 6710–6725, doi:10.1002/jgrd.50272, 2013.

3 De Wachter, E., Barret, B., Le Flochmoën, E., Pavelin, E., Matricardi, M., Clerbaux, C.,
4 Hadji-Lazaro, J., George, M., Hurtmans, D., Coheur, P.-F., Nédélec, P., and Cammas, J. P.:
5 Retrieval of MetOp-A/IASI CO profiles and validation with MOZAIC data, Atmos. Meas.
6 Tech., 5, 2843–2857, doi:10.5194/amt-5-2843-2012, 2012.

7 Drummond, J. R. and Mand, G. S.: The Measurements of Pollution in the Troposphere
8 (MOPITT) Instrument: Overall Performance and Calibration Requirements. J. Atmos.
9 Oceanic Technol., 13, 314–320, 1996.

10 Elguindi, N., Clark, H., Ordóñez, C., Thouret, V., Flemming, J., Stein, O., Huijnen, V.,
11 Moinat, P., Inness, A., Peuch, V.-H., Stohl, A., Turquety, S., Athier, G., Cammas, J.-P., and
12 Schultz, M.: Current status of the ability of the GEMS/MACC models to reproduce the
13 tropospheric CO vertical distribution as measured by MOZAIC, Geosci. Model Dev., 3, 501–
14 518, doi:10.5194/gmd-3-501-2010, 2010.

15 Emmons, L. K., Edwards, D. P., Deeter, M. N., Gille, J. C., Campos, T., Nédélec, P.,
16 Novelli, P. and G. Sachse: Measurements of Pollution In The Troposphere (MOPITT)
17 validation through 2006, Atmos. Chem. Phys., 9(5), 1795–1803, doi:10.5194/acp-9-1795-
18 2009, 2009.

19 Engelen R. J., Serrar, S., Chevallier, F.: Four-dimensional data assimilation of atmospheric
20 CO₂ using AIRS observations, J. Geophys. Res., 114, D03303, doi:10.1029/2008JD010739,
21 2009.

22 Eskes, H., Huijnen, V., Arola, A., Benedictow, A., Blechschmidt, A.-M., Botek, E., Boucher,
23 O., Bouarar, I., Chabrillat, S., Cuevas, E., Engelen, R., Flentje, H., Gaudel, A., Griesfeller, J.,
24 Jones, L., Kapsomenakis, J., Katragkou, E., Kinne, S., Langerock, B., Razinger, M., Richter,
25 A., Schultz, M., Schulz, M., Sudarchikova, N., Thouret, V., Vrekoussis, M., Wagner, A., and
26 Zerefos, C.: Validation of reactive gases and aerosols in the MACC global analysis and
27 forecast system. Geosci. Model Dev. Discuss., 8, 1117–1169, doi:10.5194/gmdd-8-1117-
28 2015, 2015.

29 Flemming, J., and Inness, A., Volcanic sulfur dioxide plume forecasts based on UV satellite
30 retrievals for the 2011 Grímsvötn and the 2010 Eyjafjallajökull eruption, Journal of
31 Geophysical Research: Atmospheres 118, 10172–10189, doi:10.1002/jgrd.50753, 2013.

1 Flemming, J., Inness, A., Flentje, H., Huijnen, V., Moinat, P., Schultz, M.G., Stein, O.:
2 Coupling global chemistry transport models to ECMWF's integrated forecast system, *Geosci.*
3 *Model Dev.*, 2, 253-265, doi:10.5194/gmd-2-253-2009, 2009.

4 Forster, P., V. Ramaswamy, P. Artaxo, T. Berntsen, R. Betts, D.W. Fahey, J. Haywood, J.
5 Lean, D.C. Lowe, G. Myhre, J. Nganga, R. Prinn, G. Raga, M. Schulz and R. Van Dorland:
6 Changes in Atmospheric Constituents and in Radiative Forcing. In: *Climate Change 2007:*
7 *The Physical Science Basis. Contribution of Working Group I to the Fourth Assessment*
8 *Report of the Intergovernmental Panel on Climate Change* [S. Solomon, D. Qin, M. Manning,
9 Z. Chen, M. Marquis, K.B. Averyt, M. Tignor and H.L. Miller (eds.)]. USA, 2007.

10 George, M., Clerbaux, C., Hurtmans, D., Turquety, S., Coheur, P.-F., Pommier, M., Hadji-
11 Lazaro, J., Edwards, D. P., Worden, H., Luo, M., Rinsland, C., and McMillan, W.: Carbon
12 monoxide distributions from the IASI/METOP mission: evaluation with other space-borne
13 remote sensors, *Atmos. Chem. Phys.*, 9, 8317–8330, doi:10.5194/acp-9-8317-2009, 2009.

14 George, M., Clerbaux, C., Bouarar, I., Coheur, P.-F., Deeter, M. N., Edwards, D. P., Francis,
15 G., Gille, C., Hadji-Lazaro, J., Hurtmans, D., Inness, A., Mao, D., Worden H. M.: An
16 examination of the long-term CO records from MOPITT and IASI and comparison of
17 retrieval methodology, *Atmos. Meas. Tech.*, 8, 4313-4328, doi:10.5194/amt-8-4313-2015,
18 2015.

19 Gomez-Pelaez, A. J., Ramos, R., Gomez-Trueba, V., Novelli, P. C., and Campo-Hernandez,
20 R.: A statistical approach to quantify uncertainty in carbon monoxide measurements at the
21 Izaña global GAW station: 2008–2011, *Atmos. Meas. Tech.*, 6, 787-799, doi:10.5194/amt-6-
22 787-2013, 2013.

23 Granier, C., Huijnen, V., Inness, A., Jones, L., Katragkou E., Khokhar, F., Kins, L., Law, K.,
24 Lefever, K., Leitao, J., Melas, D., Moinat, P., Ordonez, C., Peuch, V.-H., Reich, G., Schultz,
25 M., Stein, O., Thouret, V., Werner, T., Zerefos, C., GEMS GRG Comprehensive Validation
26 Report. Available as project report at <http://gems.ecmwf.int> (last access: February 2015),
27 2009.

28 Granier, C., Bessagnet, B., Bond, T., D'Angiola, A., van der Gon, H. D., Frost, G. J., Heil, A.,
29 Kaiser, J. W., Kinne, S., Klimont, Z., Kloster, S., Lamarque, J.-F., Liousse, C., Masui, T.,
30 Meleux, F., Mieville, A., Ohara, T., Raut, J. C., Riahi, K., Schultz, M. G., Smith, S. J.,
31 Thompson, A., van Aardenne, J., van der Werf, G. R., and van Vuuren, D. P.: Evolution of
32 anthropogenic and biomass burning emissions of air pollutants at global and regional scales

during the 1980–2010 period, *Climatic Change*, 109, 163–190, doi:10.1007/s10584-011-0154-1, 2011.

Griffin, R.J., Chen, J., Carmody, K. and Vutukuru, S.: Contribution of gas phase oxidation of volatile organic compounds to atmospheric carbon monoxide levels in two areas of the united States. *J. Geophys. Res.*, 11, D10S17, doi:10.1029/2006JD007602, 2007.

Guenther, A., Karl, T., Harley, P., Wiedinmyer, C., Palmer, P.I., and Geron, C.: Estimates of global terrestrial isoprene emissions using MEGAN (Model of Emissions of Gases and Aerosols from Nature), *Atmos. Chem. Phys.*, 6, 3181-3210, doi:10.5194/acp-6-3181-2006, 2006.

He, Y, Uno, I., Wang, Z., Ohara, T., Sugimoto, N., Shimizu, A., Richter, A., Burrows, J. P.: Variations of the increasing trend of tropospheric NO₂ over central east China during the past decade, *Atmospheric Environment*, 41, 4865–4876, 2007.

Hilboll, A., Richter, A., and Burrows, J.P.: Long-term changes of tropospheric NO₂ over megacities derived from multiple satellite instruments, *Atmos. Chem. Phys.*, 13, 4145-4169, doi:10.5194/acp-13-4145-2013, 2013a.

Hilboll, A., Richter, A., Rozanov, A., Hodnebrog, Ø., Heckel, A., Solberg, S., Stordal, F., and Burrows, J.P.: Improvements to the retrieval of tropospheric NO₂ from Satellite – stratospheric correction using SCIAMACHY limb/nadir matching and comparison to Oslo CTM2 simulations. *Atmos. Meas. Tech.*, 6, 565–584. doi:10.5194/amt-6-565-2013, 2013, 2013b.

Hollingsworth, A., Engelen, R.J., Benedetti, A., Dethof, A., Flemming, J., Kaiser, J.W., Simmons, A.J.: Toward a monitoring and forecasting system for atmospheric composition: The GEMS project, *B.Am. Meteor. Soc.*, 89, 1147–1164, doi:[10.1175/2008BAMS2355.1](https://doi.org/10.1175/2008BAMS2355.1), 2008.

Hudman, R.C., Murray, L.T., Jacob, D.J., Millet, D.B., Turquety, S., Wu, S., Blake, D.R., Goldstein, A.H., Holloway, J., Sachse, G.W.: Biogenic versus anthropogenic sources of CO over the United States. *Geophys. Res. Let.*, 35, L04801, doi:10.1175/2007GL032393, 2008.

Huijnen, V., Williams, J., vanWeele, M., van Noije, T., Krol, M., Dentener, F., Segers, A., Houweling, S., Peters, W., de Laat, J., Boersma, F., Bergamaschi, P., van Velthoven, P., Le Sager, P., Eskes, H., Alkemade, F., Scheele, R., Nédélec, P., and Pätz, H.-W.: The global

chemistry transport model TM5: description and evaluation of the tropospheric chemistry version 3.0, *Geosci. Model Dev.*, 3, 445–473, doi:10.5194/gmd-3-445-2010, 2010.

Huijnen, V., Flemming, J., Kaiser, J. W., Inness, A., Leitao, J., Heil, A., Eskes, H. J., Schultz, M. G., Benedetti, A., Dufour, G., and Eremenko, M., Hindcast experiments of tropospheric composition during the summer 2010 fires over Western Russia, *Atmos. Chem. Phys.* **12**, 4341–4364, doi:10.5194/acp-12-4341-2012, 2012.

Hurtmans, D., Coheur, P.-F., Wespes, C., Clarisse, L., Scharf, O., Clerbaux, C., Hadji-Lazaro, J., George, M., and Turquety, S.: FORLI radiative transfer and retrieval code for IASI. *J Quant Spectrosc Radiat Transfer*, 113, 1391–1408, doi:10.1016/j.jqsrt.2012.02.036, 2012.

Inness, A., Flemming, J., Suttie, M. and Jones, L.: GEMS data assimilation system for chemically reactive gases. ECMWF RD Tech Memo 587. Available from <http://www.ecmwf.int>. (last access: February 2015), 2009.

Inness, A., F. Baier, F., 2, Benedetti, A., Bouarar, I., Chabrillat, S., Clark, H., Clerbaux, C., Coheur, P., Engelen, R. J., Errera, Q., Flemming, J., George, M., Granier, C., Hadji-Lazaro, J., Huijnen, V., Hurtmans, D., Jones, L., Kaiser, J. W., Kapsomenakis, J., Lefever, K., Leitão J., Razinger, M., Richter, A., Schultz, M. G., Simmons, A. J., Suttie, M., Stein O., Thépaut J.-N., Thouret, V., Vrekoussis, M., Zerefos, C. .al.: The MACC reanalysis: an 8 yr data set of atmospheric composition, *Atmos. Chem. Phys.* **13**, 4073–4109, doi:10.5194/acp-13-4073-2013, 2013.

Inness, A., Blechschmidt, A.-M., Bouara, I., Chabrillat, S., Crepulja, M., Engelen, R. J., Eskes, H., Flemming, J., Gaudel, A., Hendrick, F., Huijnen, V., Jones, L., Kapsomenakis, J., Katragkou, E., Keppens, A., Langerock, B., de Mazière, M., Melas, D., M. Parrington, V.H. Peuch, M. Razinger, A. Richter, M.G. Schultz, M. Suttie, V. Thouret, Vrekoussis, M., Wagner, A., and Zerefos C.: Data assimilation of satellite retrieved ozone, carbon monoxide and nitrogen dioxide with ECMWF's Composition-IFS. *Atmos. Chem. Phys.*, **15**, 1–29, 2015. doi:10.5194/acp-15-1-2015.

Itahashi, S., Uno, I., Irie, H., Kurokawa, J.-I., and Ohara, T.: Regional modeling of tropospheric NO₂ vertical column density over East Asia during the period 2000–2010: comparison with multisatellite observations, *Atmos. Chem. Phys.*, **14**, 3623–3635, doi:10.5194/acp-14-3623-2014, 2014.

1 Kaiser, J. W., Heil, A., Andreae, M. O., Benedetti, A., Chubarova, N., Jones, L., Morcrette,
2 J.-J., Razinger, M., Schultz, M. G., Suttie, M., and van der Werf, G. R.: Biomass burning
3 emissions estimated with a global fire assimilation system based on observed fire radiative
4 power. *Biogeosciences*, 9, 527–554, doi:10.5194/bg-9-527-2012, 2012.

5 Kalnay, E., M. Kanamitsu, R. Kistler, W. Collins, D. Deaven, L. Gandin, M. Iredell, S. Saha,
6 G. White, J. Woollen, Y. Zhu, M. Chelliah, W. Ebisuzaki, W. Higgins, J. Janowiak, K. C.
7 Mo, C. Ropelewski, J. Wang, A. Leetmaa, R. Reynolds, R. Jenne, and D. Joseph: The
8 NCEP/NCAR 40-Year Reanalysis Project. *Bull. Amer. Meteor. Soc.*, 77, 437–471,
9 doi:[http://dx.doi.org/10.1175/1520-0477\(1996\)077<0437:TNYRP>2.0.CO;2](http://dx.doi.org/10.1175/1520-0477(1996)077<0437:TNYRP>2.0.CO;2), 1996.

10 Kalnay, E.: *Atmospheric Modeling, Data Assimilation and Predictability*. Cambridge
11 University Press, 2003.

12 Kampa, M. and Castanas, E.: Human health effects of air pollution. *Environmental*
13 *Pollution* Volume 151, Issue 2, 362–367, 2008.

14 Kerzenmacher, T., Dils, B., Kumps, N., Blumenstock, T., Clerbaux, C., Coheur, P.-F.,
15 Demoulin, P., García, O., George, M., Griffith, D. W. T., Hase, F., Hadji-Lazaro, J.,
16 Hurtmans, D., Jones, N., Mahieu, E., Notholt, J., Paton-Walsh, C., Raffalski, U., Ridder, T.,
17 Schneider, M., Servais, C., and De Mazière, M.: Validation of IASI FORLI carbon monoxide
18 retrievals using FTIR data from NDACC, *Atmos. Meas. Tech.*, 5, 2751–2761,
19 doi:10.5194/amt-5-2751-2012, 2012.

20 Kinnison, D. E., Brasseur, G. P., Walters, S., Gracia, R. R., Marsh, D. R., Sassi, F., Harvey,
21 V. L., Randall, C.E., Emmons, L., Lamarque, J. F., Hess, P., Orlando, J. J., Tie, X. X.,
22 Randel, W., Pan, L. L., Gettelman, A., Granier, C., Diehl, T., Niemeier, U. and Simmons, A.
23 J.: Sensitivity of chemical tracers to meteorological parameters in the MOZART-3 chemical
24 transport model. *J. Geophys. Res.*, 112, D20302, doi:10.1029/2006JD007879, 2007.

25 Lefever, K., van der A, R., Baier, F., Christophe, Y., Errera, Q., Eskes, H., Flemming, J.,
26 Inness, A., Jones, L., Lambert, J.-C., Langerock, B., Schultz, M. G., Stein, O., Wagner, A.,
27 and Chabrillat, S.: Copernicus atmospheric service for stratospheric ozone: validation and
28 intercomparison of four near real-time analyses, 2009–2012, *Atmos. Chem. Phys. Discuss.*,
29 14, 12461–12523, doi:10.5194/acpd-14-12461-2014, 2014.

1 Leitão, J., Richter, A., Vrekoussis, M., Kokhanovsky, A., Zhang, Q. J., Beekmann, M., and
2 Burrows, J. P.: On the improvement of NO₂ satellite retrievals – aerosol impact on the airmass
3 factors, *Atmos. Meas. Tech.*, 3, 475-493, doi:10.5194/amt-3-475-2010, 2010.

4 Leue, C., Wenig, M., Wagner, T., Platt, U. & Jähne, B. Quantitative analysis of NO_x
5 emissions from GOME satellite image sequences. *J. Geophys. Res.*, 106, 5493–5505, 2001.

6 Massart, S., Agusti-Panareda, A., Aben, I., Butz, A., Chevallier, F., Crevosier, C., Engelen,
7 R., Frankenberg, C., and Hasekamp, O.: Assimilation of atmospheric methane products into
8 the MACC-II system: from SCIAMACHY to TANSO and IASI. *Atmos. Chem. Phys.*, 14,
9 6139-6158, doi:10.5194/acp-14-6139-2014, 2014.

10 Mohnen, V.A., Goldstein, and Wang, W.-C.: Tropospheric Ozone and Climate Change, *Air &*
11 *Waste*, 43:10, 1332-1334, doi:10.1080/1073161X.1993.10467207, 1993.

12 Morcrette, J.-J., Boucher, O., Jones, L., Salmond, D., Bechthold, P., Beljaars, A., Benedetti,
13 A., Bonet, A., Kaiser, J.W., Razinger, M., Schulz, M., Serrar, S., Simmons, A.J., Sofiev, M.,
14 Suttie, M., Tompkins, A.M., Untch, A.: Aerosol analysis and forecast in the European Centre
15 for Medium- Range Weather Forecasts Integrated Forecast System: forward modeling, *J.*
16 *Geophys. Res.*, 114, D06206, doi:10.1029/2008JD011235, 2009.

17 Naik, V., Voulgarakis, A., Fiore, M., Horowitz, L.W., Lamarque, J.-F., Lin, M., Prather, M.
18 J., Young, P. J., Bergmann, D., Cameron-Smith, P. J., Cionni I., Collins W. J., Dalsøren, S.
19 B., Doherty, R., Eyring V., Faluvegi, G., Folberth, G. A., Josse, B., Lee, Y. H., MacKenzie, I.
20 A., Nagashima, T., van Noije, T. P. C., Plummer, D. A., Righi, M., Rumbold, S. T., Skeie, R.
21 D., Shindell, T., Stevenson, D. S., Strode, S., Sudo, K., Szopa, S., and Zeng, G. : Preindustrial
22 to present-day changes in tropospheric hydroxyl radical and methane lifetime from the
23 Atmospheric Chemistry and Climate Model Intercomparison Project (ACCMIP). *Atmos.*
24 *Chem. Phys.*, 13, 5277–5298, doi:10.5194/acp-13-5277-2013, 2013.

25 Novelli, P.C., Masarie, K.A. and Lang, P.M.: Distributions and recent changes of carbon
26 monoxide in the lower troposphere, *J. Geophys. Res.*, 103, 19015-19033,
27 doi:10.1029/98JD01366, 1998.

28 Ordoñez, C., Elguindi, N., Huijnen, V., Flemming, J., inness, A., Flentje, H., Katragkou, E.,
29 Moinat, P., Peuch, V.-H., Segers, A., Thouret, V., Athier, G., van Weele, M., Zerefos, C.s.,
30 Cammas, J.-P., Schulz, M.G.: Global Model simulations of air pollution during the 2003
31 European heat wave. *Atmos. Chem. Phys.*, 10, 789-815, doi:10.5194/acp-10-789-2010, 2010.

1 Park, R.J., Pickering, K.E., Allen, D. J : Global simulation of tropospheric ozone using the
2 University of Maryland Chemical Transport Model (UMD-CTM): 1. model description and
3 evaluation. *J. Geophys. Res.*, 109, doi:10.1029/2003JD004266, 2004.

4 Penkett, S., Gilge, S., Plass-Duelmer, C. Galbally, I.: WMO/GAW Expert Workshop on
5 Global Long-term Measurements of Nitrogen Oxides and Recommendations for GAW
6 Nitrogen Oxides Network, WMO, Geneva, 2011.

7 Platt, U., and Stutz, J.: Differential Optical Absorption Spectroscopy. *Physics of Earth and*
8 *Space Environments*. Berlin: Springer, [http://www.springerlink.com/content/978-3-540-](http://www.springerlink.com/content/978-3-540-21193-8)
9 [21193-8](http://www.springerlink.com/content/978-3-540-21193-8) (last access: February. 2015), 2008.

10 Richter, A., and Burrows, J.P.: “Tropospheric NO₂ from GOME Measurements.” *Advances in*
11 *Space Research* 29, no. 1, 1673–1683. doi:10.1016/S0273-1177(02)00100-X, 2002.

12 Richter, A., Burrows, J. P., Nüß, H., Granier, C, Niemeier, U.: Increase in tropospheric
13 nitrogen dioxide over China observed from space, *Nature*, 437-132,doi:10.1038/nature04092,
14 2005.

15 Richter, A. Begoin, M., Hilboll, A., and Burrows, J. P.: An improved NO₂ retrieval for the
16 GOME-2 satellite instrument, *Atmos. Meas. Tech.*, 4, 1147-1159, doi:10.5194/amt-4-1147-
17 2011, 2011.

18 Rodgers, C. D.: *Inverse Methods for Atmospheric Sounding, Theory and Practice*, World
19 Scientific, Singapore, 2000.

20 Rozanov, A., Vladimir V., Rozanov, M., Buchwitz, A., Kokhanovsky, A. and Burrows, J.P.:
21 “SCIATRAN 2.0 - A New Radiative Transfer Model for Geophysical Applications in the
22 175-2400 Nm Spectral Region.” *Advances in Space Research* 36, no. 5: 1015–1019.
23 doi:10.1016/j.asr.2005.03.012, 2005.

24 Santer, B. D., Sausen, R., Wigley, T. M. L. , Boyle, J. S. , AchutaRao, K., Doutriaux, C.,
25 Hansen, J. E, Meehl, G. A. , Roeckner, E., Ruedy, R., Schmidt, G., Taylor, K. E.: Behavior of
26 tropopause height and atmospheric temperature in models, reanalyses, and observations:
27 Decadal changes, *J. Geophys. Res.*, 108(D1), 4002, doi:10.1029/2002JD002258, 2003.

28 Savage, N. H., Agnew, P., Davis, L. S., Ordonez, C., Thorpe, R., Johnson, C. E., O’Connor,
29 F. M., and Dalvi, M.: Air quality modelling using the Met Office Unified Model (AQUUM
30 OS24-26): model description and initial evaluation, *Geosci. Model Dev.*, 6, 353–372, 2013,
31 doi:10.5194/gmd-6-353- 2013, 2013.

1 Schaap, M., Renske, M. A., Timmermans, M. R., Boersen, G. A. C., Builtjes, P. J. H.: The
2 LOTOS–EUROS model: description, validation and latest developments, *Int. J. Environ.*
3 *Pollut.*, 32, No. 2, 270–290, 2008.

4 Schreier, S. F., Richter, A., Kaiser, J. W., and Burrows, J. P.: The empirical relationship
5 between satellite-derived tropospheric NO₂ and fire radiative power and possible implications
6 for fire emission rates of NO_x, *Atmos. Chem. Phys.*, 14, 2447–2466, doi:10.5194/acp-14-
7 2447-2014, 2014.

8 Schultz, M.G., Backman, L., Balkanski, Y., Bjoerndalsaeter, S., Brand, R., Burrows, J.P.,
9 Dalsoeren, S., de Vasconcelos, M., Grodtmann, B., Hauglustaine, D.A., Heil, A.,
10 Hoelzemann, J.J., Isaksen, I.S.A., Kaurola, J., Knorr, W., Ladstaetter-Weissenmayer, B.,
11 Mota, A., Oom, D., Pacyna, J., Panasiuk, D., Pereira, J.M.C., Pulles, T., Pyle, J., Rast, S.,
12 Richter, A., Savage, N., Schnadt, C., Schulz, M., Spessa, A., Staehelin, J., Sundet, J.K.,
13 Szopa, S., Thonicke, K., van het, Bolscher M., van Noije, T. , van Velthoven, P., Vik, A.F.,
14 Wittrock, F. (2007): REanalysis of the TROpospheric chemical composition over the past 40
15 years (RETRO) — A long-term global modeling study of tropospheric chemistry, Final
16 Report Jülich/ Hamburg, Germany, published as report no. 48/2007 in the series „Reports on
17 Earth System Science“ of the Max Planck Institute for Meteorology, Hamburg, ISSN 1614-
18 1199, 2007.

19 Seinfeld, J. H., and Pandis, S. N.: *Atmospheric Chemistry and Physics: From Air Pollution to*
20 *Climate Change*, John Wiley, Hoboken, N. J., 2006.

21 Selin, N.E., Wu, S., Reilly, J. M., Paltsev, S., Prinn, R.G. and Webster, M.D.: Global health
22 and economic impacts of future ozone pollution. *Environ. Res. Lett.* 4, doi:10.1088/1748-
23 9326/4/4/044014, 2009.

24 Sheel, V., Sahu, L.K., Kajinu, M., Deushi, M., Stein, O., Nedelec, P.: Seasonal and
25 interannual variability of carbon monoxide based on MOZAIC observations, MACC
26 reanalysis, and model simulations over an urban site in India. *J. Geophys. Res.*, 119, 14,
27 9123–9141, 2014.

28 Shindell, D. T., et al.: Multimodel simulations of carbon monoxide: Comparison with
29 observations and projected near-future changes, *J. Geophys. Res.*, 111, D19306,
30 doi:10.1029/2006JD007100, 2006.

1 Sinnhuber, B.M., Weber, M., Amankwah, A. and Burrows, J.P.: “Total Ozone during the
 2 Unusual Antarctic Winter of 2002.” *Geophysical Research Letters* 30, no. 11, 1580–1584.
 3 doi:10.1029/2002GL016798, 2003.

4 Sinnhuber, M., Burrows, J.P., Chipperfield, M., P., Jackman, C. H., Kallenrode, M.-B.,
 5 Künzi, K.F., and Quack, M.: A Model Study of the Impact of Magnetic Field Structure on
 6 Atmospheric Composition during Solar Proton Events., *Geophys.. Res. Lett.*, 30, 1818–1821,
 7 doi:10.1029/2003GL017265, 2003.

8 S. Sitch, S., Cox, P. M., Collins, W. J., Huntingford, C.: Indirect radiative forcing of climate
 9 change through ozone effects on the land-carbon sink. *Nature* 448, 791-794,
 10 doi:10.1038/nature06059, 2007.

11 Stein, O., Schultz, M. G., Flemming, J., Inness, A., Kaiser, J., Jones, L., Benedetti, A.,
 12 Morcrette, J.-J.: MACC Global air quality services – Technical Documentation. MACC
 13 project deliverable D_G-RG_3.8, available at:
 14 www.gmes-atmosphere.eu/documents/deliverables/g-rg/ (last access: February 2015), 2011.

15 Stein, O., Flemming, J., Inness, A., Kaiser, J. W., and Schultz, M. G.: Global reactive gases
 16 and reanalysis in the 5 MACC project, *J. Integr. Environ. Sci.*,
 17 doi:10.1080/1943815X.2012.696545, 2012.

18 Stein, O., Huijnen, V., Flemming, J.: Model description of the IFS-MOZART and IFS-TM5
 19 coupled systems. MACC-II project deliverable D_55.4, available at:
 20 <https://www.gmes-atmosphere.eu/documents/maccii/deliverables/grg/> (last access: February
 21 2015), 2013.

22 Stein, O., Schultz, M. G., Bouarar, I., Clark, H., Huijnen, V., Gaudel, A., George, M., and
 23 Clerbaux, C.: On the wintertime low bias of Northern Hemisphere carbon monoxide found in
 24 10 global model simulations, *Atmos. Chem. Phys.*, 14, 9295–9316, doi:10.5194/acp-14-9295-
 25 2014, 2014.

26 Tørseth, K., Aas, W., Breivik, K., Fjæraa, A. M., Fiebig, M., Hjellbrekke, A. G., Lund
 27 Myhre, C., Solberg, S., and Yttri, K. E.: Introduction to the European Monitoring and
 28 Evaluation Programme (EMEP) and observed atmospheric composition change during
 29 1972–2009, *Atmos. Chem. Phys.*, 12, 5447-5481, doi:10.5194/acp-12-5447-2012, 2012.

1 Valcke, S., Redler, R.: OASIS4 User Guide (OASIS4_0_2). PRISM–Support Initiative,
2 Technical Report No 4, available at:
3 http://www.prism.enes.org/Publications/Reports/OASIS4_User_Guide_T4.pdf (last access:
4 February 2015), 2006.

5 Val Martin, M., Heald, C.L., Arnold, S.R.: Coupling dry deposition to vegetation phenology
6 in the Community Earth System Model: Implications for the simulation of surface O₃.
7 *Geophys Res. Lett.*, 41, 2988–2996, doi:10.1002/2014GL059651, 2014.

8 Van der Werf, G. R., Randerson, J. T., Giglio, L., Collatz, G. J., and Kasibhatla, P. S.:
9 Interannual variability in global biomass burning emissions from 1997 to 2004. *Atmos.*
10 *Chem. Phys.*, 6(11):3423–3441, doi:10.5194/acp-6-3423-2006, 2006.

11 Velders, G. J. M., Granier, C., Portmann, R. W., Pfeilsticker, K., Wenig, M., Wagner, T.,
12 Platt, U., Richter, A., and Burrows, J. P.: Global tropospheric NO₂ column distributions:
13 Comparing 3-D model calculations with GOME measurements, *J. Geophys. Res.*, 106,
14 12643– 12660, 2001.

15 Wang, P., Stammes, P., van der A, R., Pinardi, G., and van Roozendael, M.: FRESCO+: An
16 improved O₂ A-band cloud retrieval algorithm for tropospheric trace gas retrievals, *Atmos.*
17 *Chem. Phys.*, 8, 6565–6576, doi:10.5194/acp-8-6565-2008, 2008.

18 Winkler, H., Sinnhuber, M., Notholt, J., Kallenrode, M.B., Steinhilber, F., Vogt, J., Zieger,
19 B., Glassmeier, K.H. and Stadelmann, A.: Modeling impacts of geomagnetic field variations
20 on middle atmospheric ozone responses to solar proton events on long timescales, *J. Geophys.*
21 *Res.* 113, D02302, doi:10.1029/2007JD008574, 2008.

22 WMO:WMO Global Atmosphere Watch (GAW) Strategic Plan: 2008 – 2015. World
23 Meteorological Organization, Geneva, Switzerland, 2007.

24 WMO: Guidelines for the Measurement of Atmospheric Carbon Monoxide, GAW Report No.
25 192, World Meteorological Organization, Geneva, Switzerland, 2010.

26 WMO: WMO/GAW Expert Workshop on Global Long-term Measurements of Nitrogen
27 Oxides and Recommendations for GAW Nitrogen Oxides Network, GAW Report No. 195,
28 World Meteorological Organization, Geneva, Switzerland, 2011.

29

- 1 WMO: 16th WMO/IAEA Meeting on Carbon Dioxide, Other greenhouse Gases and Related
2 Measurement Techniques (GGMT-2011), Geneva, 2012.
- 3 WMO : Guidelines for the Continuous Measurements of Ozone in the
4 Troposphere, GAW Report No. 209, World Meteorological Organization, Geneva,
5 Switzerland, 2013.
- 6 Worden, H. M., Deeter, M. N., Edwards, D. P., Gille, J. C., Drummond, J. R. and Nedelec, P.
7 P.: Observations of near-surface carbon monoxide from space using MOPITT multispectral
8 retrievals, J. Geophys. Res., 115, doi:10.1029/2010JD014242, 2010.
- 9 Worden, H. M., Deeter, M. N., Edwards, D. P., Gille, J., Drummond, J., Emmons, L. K.,
10 Francis, G., Martínez-Alonso, S.: 13 years of MOPITT operations: lessons from MOPITT
11 retrieval algorithm development, Ann. Geophys., 56,, doi:10.4401/ag-6330, 2014.

1 Table 1: List of assimilated data in the MACC_osuite

Instrument	Satellite	Provider	Version	Type	Status
MLS	AURA	NASA	V02	O ₃ Profiles	20090901 - 20121231
OMI	AURA	NASA	V883	O ₃ Total column	20090901 - 20121231
SBUV-2	NOAA	NOAA	V8	O ₃ 6 layer profiles	20090901 - 20121231
SCIAMACHY	Envisat	KNMI		O ₃ total column	20090916 - 20120408
IASI	MetOp-A	LATMOS/ULB		CO Total column	20090901 - 20121231
MOPITT	TERRA	NCAR	V4	CO Total column	20120705 - 20121231
OMI	AURA	KNMI	DOMINO V2.0	NO ₂ Tropospheric column	20120705 - 20121231
OMI	AURA	NASA	v003	SO ₂ Tropospheric column	20120705 - 20121231
MODIS	AQUA / TERRA	NASA	Col. 5	Aerosol total optical depth	20090901 - 20121231

2

1

2 Table 2: Description of the set-up of the MACC_osuite between 9/2009 and 12/2012. Details
3 on the assimilated data are provided in Table 1. A description of the emissions is given in
4 section 2.1.1 in the text.

Model Cycle	CTM	Assimilated Data	Emissions
CY36R1	MOZART v3.0	O ₃ (MLS, OMI, SBUV-2 SCIAMACHY), CO (IASI)	RETRO / REAS / GEIA / GFEDv2/GFAS
CY37R3	MOZART v3.5	O ₃ (MLS, OMI, SBUV-2), CO (IASI, MOPITT), NO ₂ (OMI), SO ₂ (OMI)	MACCity / MEGAN / GFASv1.0 daily

5

- 1 Table 3: List of GAW and EMEP stations used in the evaluation (GAW listed by label, EMEP
- 2 listed by region: Northern Europe NE, Central Europe CE and Southern Europe SE).The
- 3 numbers behind the name provide the type of gas: 1=O₃, 2=CO, 3=NO₂.

Station	Label/Region	Programme	Lat	Lon	Alt [m a.s.l.]	Station	Label/Region	Programme	Lat	Lon	Alt [m a.s.l.]
Ähtäri II ¹	NE	EMEP	62.58	24.18	180	Masenbergl ¹	CE	EMEP	47.35	15.88	1170
Alert ²	ALT	GAW	82.45	-62.52	210	Mauna Loa ¹	MAU	GAW	19.54	-155.58	3397
Arrival Heights ¹	ARH	GAW	-77.80	166.67	184	Minamitorishima ^{1,2}	MNM	GAW	24.29	153.98	8
Aspvreten ¹	NE	EMEP	58.80	17.38	20	Montandon ¹	CE	EMEP	47.30	6.83	836
Assekrem ¹	ASS	GAW	23.27	5.63	2710	Monte Cimone ^{1,2}	MCI	GAW	44.18	10.70	2165
Aston Hill ¹	NE	EMEP	52.50	-3.03	370	Monte Velho ¹	SE	EMEP	38.08	-8.80	43
Auchencorth ¹	NE	EMEP	55.79	-3.24	260	Montelibretti ¹	CE	EMEP	42.10	12.63	48
Ayia Marina ¹	SE	EMEP	35.04	33.06	532	Montfranc ¹	CE	EMEP	45.80	2.07	810
Barcarrola ¹	SE	EMEP	38.47	-6.92	393	Morvan ¹	CE	EMEP	47.27	4.08	620
Baring Head ¹	BAH	GAW	-41.41	174.87	85	Narberth ¹	NE	EMEP	51.23	-4.70	160
Barrow ¹	BAR	GAW	71.32	-156.60	11	Neuglobsow ^{1,2}	NGW/NE	GAW/EMEP	53.17	13.03	62
BEO Moussala ^{1,2}	BEO	GAW	42.18	23.59	2925	Neumayer ¹	NEU	GAW	-70.65	-8.25	42
Birkenes ¹	NE	EMEP	58.38	8.25	190	Niembro ¹	CE	EMEP	43.44	-4.85	134
Bredkälen ¹	NE	EMEP	63.85	15.33	404	Norra-Kvill ¹	NE	EMEP	57.81	15.56	261
Bush ¹	NE	EMEP	55.86	-3.21	180	O Saviñao ¹	CE	EMEP	43.23	-7.70	506
Cabauw ¹	NE	EMEP	51.97	4.92	60	Offagne ¹	CE	EMEP	49.88	5.20	430
Cabo de Creus ¹	CE	EMEP	42.32	3.32	23	Oulanka ¹	NE	EMEP	66.32	29.40	310
Cairo ¹	CAI	GAW	30.08	31.28	35	Pallas ¹	NE	EMEP	68.00	24.15	340
Campisabalos ¹	CE	EMEP	41.28	-3.14	1360	Payerne ^{1,2}	PAY/CE	GAW/EMEP	46.81	6.94	510
Cape Grim ¹	CAG	GAW	-40.68	144.68	94	Penausende ¹	CE	EMEP	41.28	-5.86	985
Cape Point ^{1,2}	CAP	GAW	-34.35	18.48	230	Peyrusse Vieille ¹	CE	EMEP	43.62	0.18	200
Cape Verde ^{1,2}	CVO	GAW	16.85	-24.87	10	Pic du Midi ^{1,2}	PIC/CE	GAW/EMEP	42.94	0.14	2877
Charlton Mackrell ¹	NE	EMEP	51.06	-2.68	54	Pillersdor ¹	CE	EMEP	48.72	15.94	315
Chaumont ¹	CE	EMEP	47.05	6.98	1130	Preila ¹	NE	EMEP	55.35	21.07	5
Chibougamau ²	CHI	GAW	49.68	-74.34	393	Prestebakke ¹	NE	EMEP	59.00	11.53	160
Chopok ¹	CE	EMEP	48.93	19.58	2008	Puy de Dôme ^{1,2}	PUY/CE	GAW/EMEP	45.77	2.95	1465
Concordia ¹	CON	GAW	-75.10	123.33	3233	Ragged Point ¹	RAG	GAW	13.17	-59.43	45
De Zilk ¹	NE	EMEP	52.30	4.50	4	Rao ¹	NE	EMEP	57.39	11.91	10
Diabla Gora ¹	NE	EMEP	54.15	22.07	157	Revin ¹	CE	EMEP	49.90	4.63	390
Dobele ¹	DOB	GAW	56.37	23.19	42	Rigi ^{1,2,3}	RIG/CE	GAW/EMEP	47.07	8.46	1030
Doñana ¹	SE	EMEP	37.03	-6.33	5	Rojen Peak ¹	CE	EMEP	41.70	24.74	1750
Donon ¹	CE	EMEP	48.50	7.13	775	Rucava ¹	RUC/NE	GAW/EMEP	56.10	21.10	18
Dunkelsteinerwald ¹	CE	EMEP	48.37	15.55	320	Ryori ^{1,2}	RYO	GAW	39.03	141.82	260
East Trout Lake ²	ETL	GAW	54.35	-104.98	492	Sable Island ²	SAB	GAW	43.93	-60.02	5
Egbert ²	EGB	GAW	44.23	-79.78	253	San Pablo de los Montes ¹	SE	EMEP	39.55	-4.35	917
Eibergen ¹	NE	EMEP	52.08	6.57	20	Sandve ¹	NE	EMEP	59.20	5.20	15
Els Torms ¹	CE	EMEP	41.40	0.72	470	Schauinsland ^{1,2,3}	SCH/CE	GAW/EMEP	47.92	7.92	1205
Eskdalemuir ¹	NE	EMEP	55.31	-3.20	243	Schmücke ¹	NE	EMEP	50.65	10.77	937
Esrang ¹	NE	EMEP	67.88	21.07	475	Sibton ¹	NE	EMEP	52.29	1.46	46

Estevan Point ^{1,2}	ESP	GAW	49.38	-126.55	39	Śnieżka ¹	NE	EMEP	50.73	15.73	1603
Eupen ¹	NE	EMEP	51.46	6.00	295	Sonnblick ^{1,2,3}	SBL/CE	GAW/EMEP	47.05	12.96	3106
Everest - Pyramid ¹	EVP	GAW	27.96	86.82	5079	South Pole ¹	SPO	GAW	-89.98	-24.80	2810
Finokalia ¹	SE	EMEP	35.32	25.67	250	Spitsbergen ¹	NE	EMEP	78.90	11.88	474
Forstho ¹	CE	EMEP	48.10	15.91	581	St. Osyth ¹	NE	EMEP	51.78	1.08	8
Fraserdale ²	FRA	GAW	49.88	-81.57	210	Stará Lesná ¹	CE	EMEP	49.15	20.28	808
Gänserndorf ¹	CE	EMEP	48.33	16.73	161	Starina ¹	CE	EMEP	49.05	22.27	345
Gerlitz ¹	CE	EMEP	46.69	13.92	1895	Stixneusiedl ¹	CE	EMEP	48.05	16.68	240
Graz Platte ¹	CE	EMEP	47.11	15.47	651	Strath Vaich Dam ¹	NE	EMEP	57.73	-4.77	270
Great Dun Fell ¹	NE	EMEP	54.68	-2.45	847	Summit ¹	SUM	GAW	72.58	-38.48	3238
Greibenzen ¹	CE	EMEP	47.04	14.33	1648	Svratouch ¹	CE	EMEP	49.73	16.05	737
Grimsoe ¹	NE	EMEP	59.73	15.47	132	Syowa Station ¹	SYO	GAW	-69.00	39.58	16
Harwell ¹	NE	EMEP	51.57	-1.32	137	Tänikon ¹	CE	EMEP	47.48	8.90	540
Haunsberg ¹	CE	EMEP	47.97	13.02	730	Topolniky ¹	CE	EMEP	47.96	17.86	113
Heidenreichstein ¹	CE	EMEP	48.88	15.05	570	Trinidad Head ¹	TRI	GAW	41.05	-124.15	120
High Muffles ¹	NE	EMEP	54.33	-0.80	267	Tsukuba ¹	TSU	GAW	36.05	140.13	25
Hurdal ¹	NE	EMEP	60.37	11.08	300	Tudor Hill ¹	TUD	GAW	32.27	-64.87	30
Illmitz ¹	CE	EMEP	47.77	16.77	117	Tustervatn ¹	NE	EMEP	65.83	13.92	439
Iskrba ¹	ISK/CE	GAW/EMEP	45.56	14.86	520	Tutuila ¹	TUT	GAW	-14.24	-170.57	42
Izaña (Tenerife) ^{1,2}	IZO	GAW	28.30	-16.50	2367	Ushuaia ^{1,2}	USH	GAW	-54.85	-68.32	18
Jarczew ¹	NE	EMEP	51.82	21.98	180	Utö ¹	NE	EMEP	59.78	21.38	7
Jungfrauoch ^{1,2,3}	JFJ/CE	GAW/EMEP	46.55	7.99	3578	Vavihill ¹	NE	EMEP	56.01	13.15	175
Karasjok ¹	NE	EMEP	69.47	25.22	333	Vezin ¹	NE	EMEP	50.50	4.99	160
Keldsno ¹	NE	EMEP	54.73	10.73	10	Vilsandi ¹	NE	EMEP	58.38	21.82	6
Kollumerwaard ^{1,2,3}	KOW/NE	GAW/EMEP	53.33	6.28	1	Vindeln ¹	VIN/NE	GAW/EMEP	64.25	19.77	225
Košetice ^{1,2,3}	KOS/CE	GAW/EMEP	49.58	15.08	534	Virolahti II ¹	NE	EMEP	60.53	27.69	4
Kovk ¹	KOV/CE	GAW/EMEP	46.12	15.11	600	Vorhegg ¹	CE	EMEP	46.68	12.97	1020
K-puszt ¹	CE	EMEP	46.97	19.58	125	Vredepeel ¹	NE	EMEP	51.54	5.85	28
Krvavec ^{1,2}	KRV/CE	GAW/EMEP	46.30	14.54	1740	Waldhof ¹	WAL/NE	GAW/EMEP	52.80	10.77	74
La Coulonche ¹	CE	EMEP	48.63	-0.45	309	Westerland ¹	WES/NE	GAW/EMEP	54.93	8.32	12
La Tardière ¹	CE	EMEP	46.65	-0.75	143	Weybourne ¹	NE	EMEP	52.95	1.12	16
Lac La Biche ²	LAC	GAW	54.95	-112.45	540	Wicken Fen ¹	NE	EMEP	52.30	-0.29	5
Ladybower Res. ¹	NE	EMEP	53.40	-1.75	420	Yarner Wood ¹	NE	EMEP	50.59	-3.71	119
Lahemaa ¹	NE	EMEP	59.50	25.90	32	Yonagunijima ^{1,2}	YON	GAW	24.47	123.02	30
Lauder ¹	LAU	GAW	-45.03	169.67	370	Zarodnje ¹	CE	EMEP	46.42	15.00	770
Le Casset ¹	CE	EMEP	45.00	6.47	750	Zarra ¹	SE	EMEP	39.09	-1.10	885
Leba ¹	NE	EMEP	54.75	17.53	2	Zavodnje ¹	ZAV	GAW	46.43	15.00	770
Lerwick ¹	NE	EMEP	60.13	-1.18	85	Zillertaler Alpen ¹	CE	EMEP	47.14	11.87	1970
Lille Valby ¹	NE	EMEP	55.69	12.13	10	Zingst ¹	ZIN/NE	GAW/EMEP	54.43	12.73	1
Lough Navar ¹	NE	EMEP	54.44	-7.87	126	Zoebelboden ¹	CE	EMEP	47.83	14.44	899
Lullington Heath ¹	NE	EMEP	50.79	0.17	120	Zoseni ¹	ZOS/NE	GAW/EMEP	57.13	25.90	188
Mace Head ¹	NE	EMEP	53.17	-9.50	15	Zugspitze ^{1,2}	SFH	GAW	47.42	10.98	2656
Market Harborough ¹	NE	EMEP	52.55	-0.77	145						

1 Table 4: Modified normalized mean bias (MNMB) [%], correlation coefficient (R), and root
2 mean square error (RMSE) [ppb] derived from the evaluation of the MACC_osuite with
3 Global Atmosphere Watch (GAW) O₃ surface observations during the period 09/2009 to
4 12/2012.

Station	ARH	ASS	BAH	BAR	BEO	CAI	CAG	CAP	CVO	CON	DOB	EVP	ISK	IZO	JFJ	KOW	KOS
MNMB	-39.8	-6.3	-8.6	-35.1	-21.4	70.1	-12.7	13.7	15.2	-81.6	6.3	18.4	67.2	10.4	1.9	5.8	-5.9
R	0.6	0.7	0.5	0.3	0.4	-0.1	0.4	0.6	0.6	0.3	0.3	0.7	0.1	0.5	0.7	0.6	0.6
RMSE	10.6	6.5	8.0	13.8	20.4	29.2	8.9	7.6	8.0	17.2	14.3	12.0	34.5	10.8	7.4	12.0	16.3

5

Station	KOV	KRV	LAU	MAU	MNM	MCI	NGW	NEU	PAY	PIC	PUY	RAG	RIG	RUC	RYO	SCH	SBL
MNMB	21.2	9.5	-5.5	13.7	38.6	2.3	-11.4	-45.2	-28.8	5.5	12.8	38.6	-80.3	-0.1	10.5	8.5	8.1
R	0.6	0.6	0.5	0.6	0.8	0.7	0.5	0.5	0.7	0.6	0.6	0.6	0.3	0.3	0.1	0.7	0.6
RMSE	19.5	11.1	9.0	11.5	13.0	8.2	14.3	11.4	15.6	7.7	10.6	10.6	28.4	15.0	14.4	12.2	9.3

6

Station	SFH	SPO	SUM	SYO	TRI	TSU	TUD	TUT	USH	VIN	WAL	WES	YON	ZAV	ZIN	ZOS
MNMB	10.1	-70.6	-24.4	-31.2	3.2	55.1	45.3	40.2	-7.0	4.6	-18.0	-12.3	22.0	19.7	-17.5	22.3
R	0.6	0.4	0.5	0.7	0.3	0.0	0.5	0.8	0.5	0.4	0.6	0.6	0.7	0.6	0.4	0.2
RMSE	9.3	16.3	11.7	8.9	13.3	27.6	18.2	8.0	7.6	11.2	13.6	11.6	13.6	18.6	13.9	17.0

7

1 Table 5: Modified normalized mean bias (MNMB) [%], correlation coefficient (R), and root
2 mean square error (RMSE) [ppb] derived from the evaluation of the MACC_osuite with
3 Global Atmospheric Watch (GAW) CO surface observations during the period 09/2009 to
4 12/2012.

Station	ALT	BEO	CAP	CHI	CVO	EGB	ESP	ETL	FRA	IZO	JFJ	KOS	KOW	KRV	LAC	MCI	MNM
MNMB	-6.9	-36.1	29.7	-7.3	-0.6	4.5	-1.7	-19.9	-12.0	-6.8	-15.1	-50.1	-5.9	-30.4	-24.2	-19.0	6.4
R	0.5	0.0	0.6	0.4	0.7	0.3	0.5	0.1	0.3	0.7	0.6	0.2	0.4	0.4	0.0	0.6	0.8
RMSE	23.4	90.3	20.4	31.1	14.2	60.1	25.7	53.9	35.9	15.3	25.8	131.1	70.1	49.1	58.5	32.0	22.0

5

Station	NGW	PAY	PIC	PUY	RIG	RYO	SAB	SBL	SCH	SFH	USH	YON
MNMB	-1.7	-7.3	-9.3	-10.4	28.2	-4.8	-8.1	-25.1	-15.8	-25.7	-9.1	-1.6
R	0.4	0.3	0.7	0.6	0.0	0.4	0.4	0.5	0.5	0.4	0.6	0.7
RMSE	61.6	99.2	18.4	30.6	143.5	44.5	31.6	36.8	39.8	45.0	12.3	62.3

6

1 Table 6: Modified normalized mean bias (MNMB) [%] derived from CO satellite
2 observations (MOPITT) and the MACC_osuite simulations of CO total columns from
3 10/2009 until 06/2012 averaged over different regions.

	Oct 09	Nov 09	Dec 09	Jan 10	Feb 10	Mar 10	Apr 10	May 10	Jun 10	Jul 10	Aug 10
Europe	4.17	1.35	-7.02	-7.17	-7.84	-8.56	-5.20	-2.15	-2.96	0.75	-2.88
Alaska	0.31	-3.16	-6.71	-8.85	-6.39	-3.13	-4.49	-3.85	-8.69	-6.18	-3.94
Siberia	2.02	1.62	-1.44	-2.75	-1.36	-2.27	-3.58	-2.93	-5.30	4.21	-8.43
N. Africa	6.53	9.17	5.82	7.05	3.45	-2.96	-3.53	-1.75	-3.40	-1.21	-3.58
S. Africa	-12.45	-9.44	3.10	6.53	8.27	6.63	3.57	2.33	7.34	0.57	-2.75
S. Asia	9.20	13.73	6.95	6.41	6.69	1.12	3.18	1.26	-3.01	1.98	2.15
E. Asia	8.04	12.33	-5.86	-9.18	-6.64	-4.49	-5.12	-5.61	-7.72	-4.34	-2.80
US	9.73	6.71	-5.42	-7.75	-10.88	-6.26	-3.80	-2.04	1.58	2.54	2.98
	Sep 10	Oct 10	Nov 10	Dec 10	Jan 11	Feb 11	Mar 11	Apr 11	May 11	Jun 11	Jul 11
Europe	-1.97	-0.92	-2.94	-7.78	-15.41	-17.22	-18.78	-17.34	-13.34	-6.62	-3.91
Alaska	-5.00	-1.89	-4.87	-7.51	-14.54	-9.90	-9.29	-12.54	-11.95	-10.04	-4.73
Siberia	-2.94	-1.93	-1.73	-3.02	-7.71	-7.78	-12.09	-21.99	-17.23	-11.59	-4.97
N. Africa	-1.22	3.33	5.98	7.03	-0.53	4.31	2.66	1.37	4.23	4.71	4.37
S. Africa	-5.13	2.84	7.39	4.37	1.41	3.39	3.80	0.99	5.71	3.45	-2.75
S. Asia	5.05	6.72	9.63	10.30	2.19	2.91	1.48	-1.76	1.68	1.62	2.90
E. Asia	6.13	6.93	2.44	3.23	-11.25	-9.18	-9.63	-8.58	-4.73	-1.62	5.00
US	0.08	-0.71	1.20	-8.06	-18.30	-16.98	-14.33	-13.52	-8.10	-4.72	-0.64
	Aug 11	Sep 11	Oct 11	Nov 11	Dec 11	Jan 12	Feb 12	Mar 12	Apr 12	May 12	Jun 12
Europe	-2.57	-7.28	-10.80	-11.85	-14.79	-13.50	-14.16	-15.30	-11.49	-7.00	-3.65
Alaska	-5.69	-11.86	-18.05	-14.33	-12.29	-11.50	-11.24	-11.92	-9.42	-8.71	-4.74
Siberia	-6.05	-15.16	-16.50	-10.32	-11.59	-10.15	-8.45	-13.14	-12.18	-11.08	-4.45
N. Africa	6.15	5.35	6.27	-0.93	3.37	2.04	1.11	-5.90	-3.40	-3.59	-0.95
S. Africa	-6.70	-4.43	-0.58	3.64	4.66	4.25	2.91	0.91	3.41	1.33	-1.23
S. Asia	3.80	2.27	4.24	4.76	7.00	3.24	1.72	-1.23	-0.90	0.49	-0.61
E. Asia	3.05	1.60	-2.60	-2.48	-5.15	-5.56	-4.63	-0.85	-0.36	-2.63	0.68
US	-1.17	-2.40	-4.23	-6.14	-10.84	-13.30	-14.87	-9.19	-6.94	-2.88	-2.55

1 Table 7: Statistics derived from satellite observations (SCIAMACHY from 09/2009 until
2 03/2012, GOME-2 from 04/2012 to 12/2012) and the MACC_osuite simulations of daily
3 tropospheric NO₂ VCD [10^{15} molec cm⁻²] averaged over different regions for September 2009
4 to December 2012.

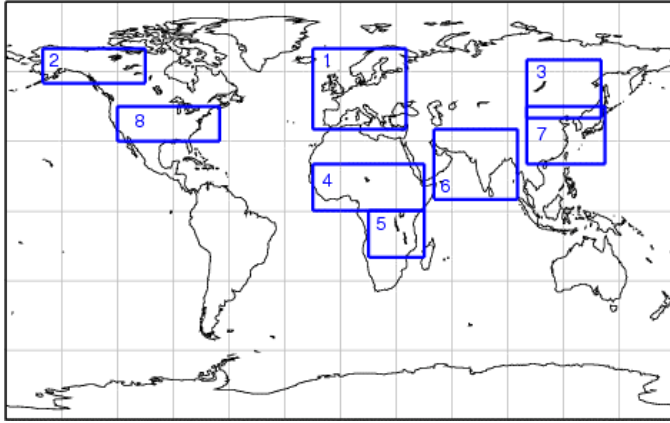
Region	United States	Europe	South Asia	East Asia	South Africa	North Africa
Model mean NO ₂ VCD [10^{15} molec cm ²]	2.6	2.1	1.0	2.4	0.8	0.9
Satellite mean NO ₂ VCD [10^{15} molec cm ²]	3.1	3.6	1.2	6.2	1.1	0.9
Modified normalized mean bias (MNMB) [%]	-17.3	-49.0	-13.4	-70.7	-36.8	-0.4
Root mean square error (RMSE) [10^{15} molec cm ²]	1.2	2.0	0.3	6.0	0.5	0.3
Correlation coefficient (R) [dimensionless]	0.6	0.8	0.8	0.8	0.6	0.5

5

1 Table 8: Modified normalized mean bias (MNMB) [%], correlation coefficient (R), and root
 2 mean square error (RMSE) [ppb] derived from the evaluation of the MACC_osuite with
 3 Global Atmospheric Watch (GAW) NO₂ surface observations during the period 09/2009 to
 4 12/2012.

Station	JFJ	KOW	KOS	RIG	SCH	SBL
MNMB	-44.7	-28.7	-38.5	68.0	-25.7	-160.6
R	0.2	0.6	0.4	0.2	0.4	0.1
RMSE	0.3	5.2	5.4	8.9	2.2	0.9

1



2

3 Figure 1: Regions used for regional data-stratification in the troposphere for the comparison
 4 with satellite data. The following regions are defined: **1** Europe (15W– 35E, 35N–70N), **2**
 5 Alaska (150W–105W, 55N–70N), **3** Siberia (100E–140E, 40N–65N), **4** North Africa (15W–
 6 45E, 0N–20N), **5** South Africa (15E–45E, 20S–0S), **6** South Asia (50E–95E, 5N–35N), **7** East
 7 Asia (100E–142E, 20N–45N), **8** United States (120W–65W, 30N–45N).

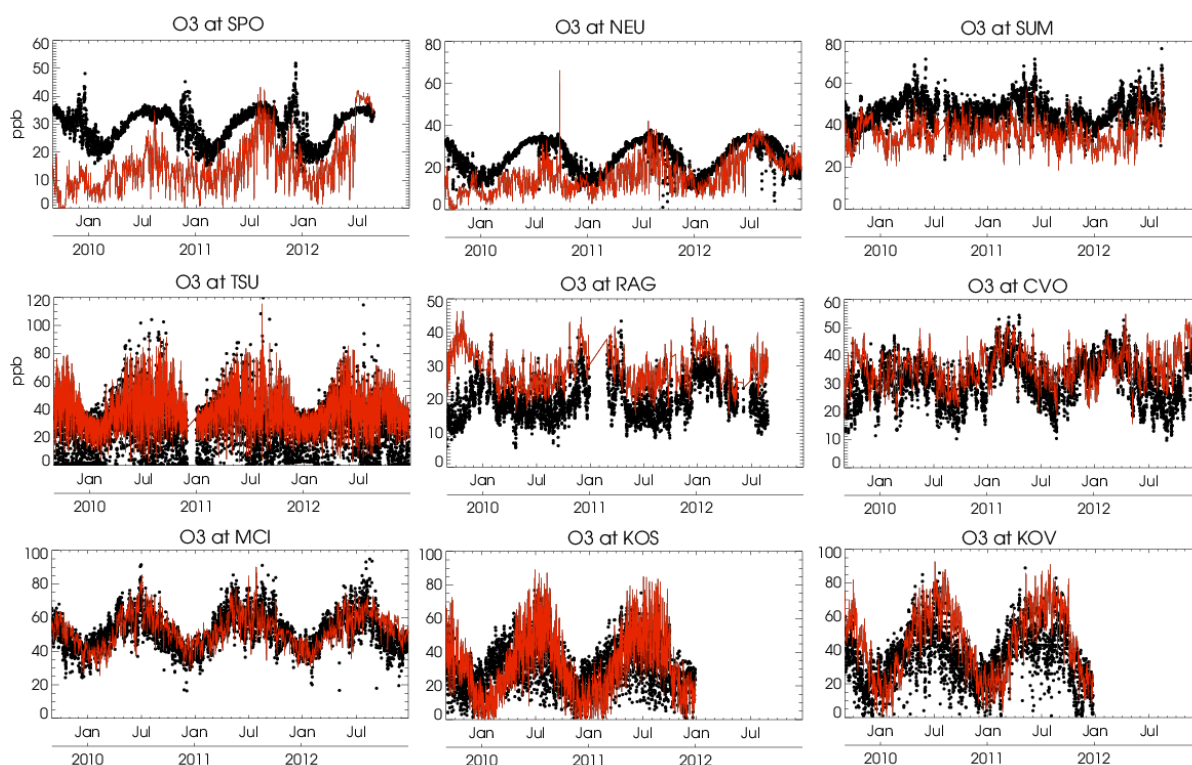
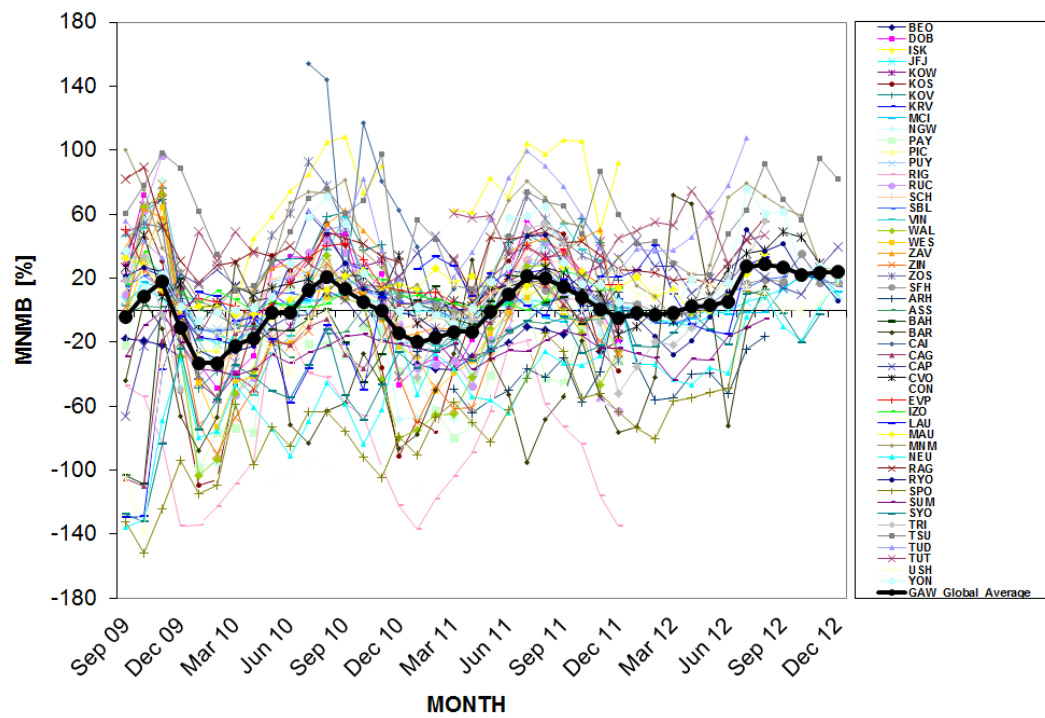
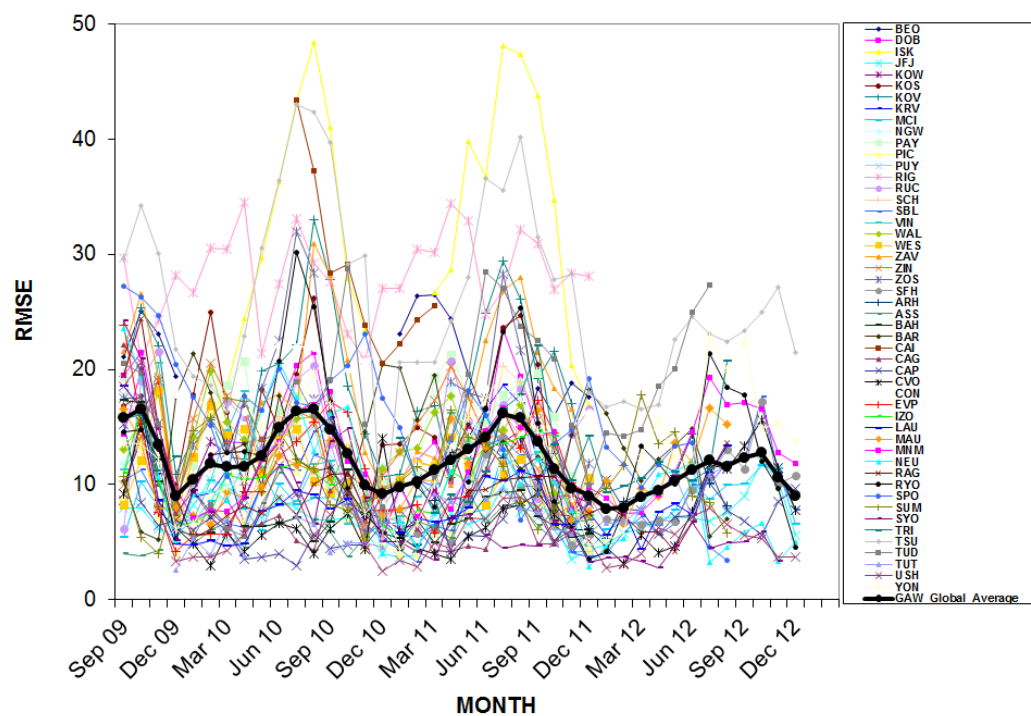


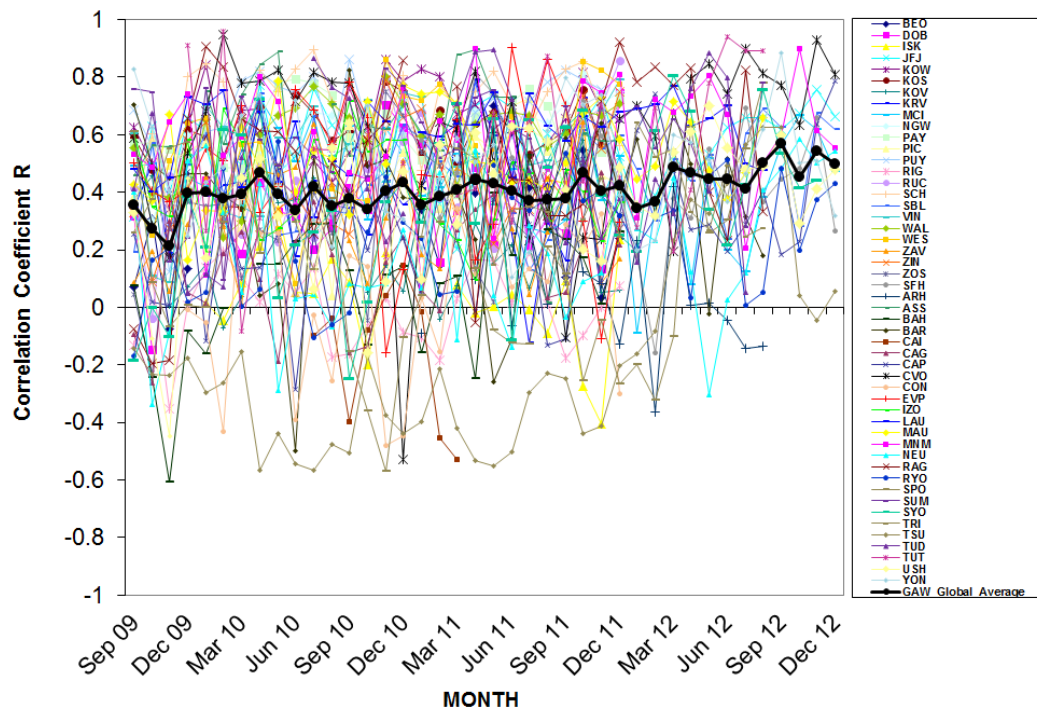
Figure 3: Time series plots of the MACC_osuite 6-hourly O₃ mixing ratios (red) and GAW surface observations (black) for South Pole-SPO (Antarctica), Neumayer-NEU (Antarctica), Summit-SUM (Denmark), Tsukuba-TSU (Japan), Ragged Point-RAG, (Barbados), Cape Verde Observatory-CVO (Cape Verde), Monte Cimone-MCI (Italy), Kosetice-KOS (Czech Republic) and Kovk- KOV(Slovenia) during the period 09/2009 to 12/2012. Unit: ppb



1
2 Figure 4: Modified normalized mean bias (MNMB) in % derived from the evaluation of the
3 MACC_osuite with GAW O₃ surface observations during the period September 2009 to
4 December 2012 (black line: global average of 50 GAW stations. Multi-coloured lines:
5 individual station results, see legend to the right).

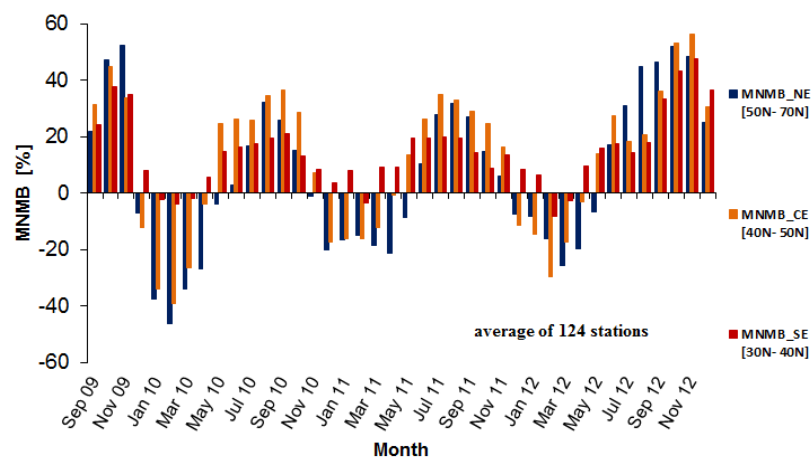


1
2 Figure 5: Root mean square error (RMSE) in ppb derived from the evaluation of the
3 MACC_osuite with GAW O₃ surface observations during the period September 2009 to
4 December 2012 (black line: global average of 50 GAW stations. Multi-coloured lines:
5 individual station results, see legend to the right).



1

2 Figure 6: Correlation coefficient (R), derived from the evaluation of the MACC_osuite with
 3 GAW O₃ surface observations during the period September 2009 to December 2012 (black
 4 line: global average of 50 GAW stations. Multi-coloured lines: individual station results, see
 5 legend to the right).



1
2 Figure 7: Modified normalized mean biases (MNMBs) derived from the evaluation of the
3 MACC_osuite with EMEP O₃ surface observations in three different parts in Europe (blue:
4 Northern Europe, orange: Central Europe, red: Southern Europe) during the period September
5 2009 to December 2012.

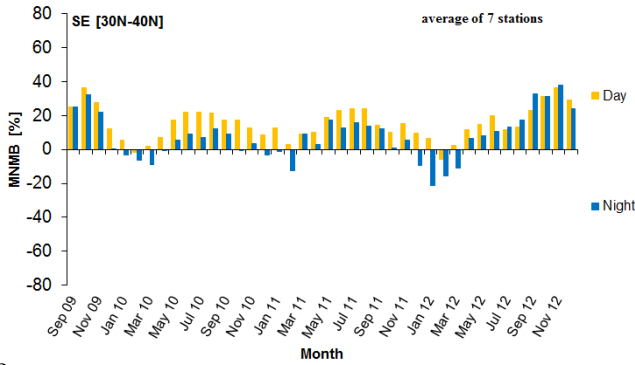
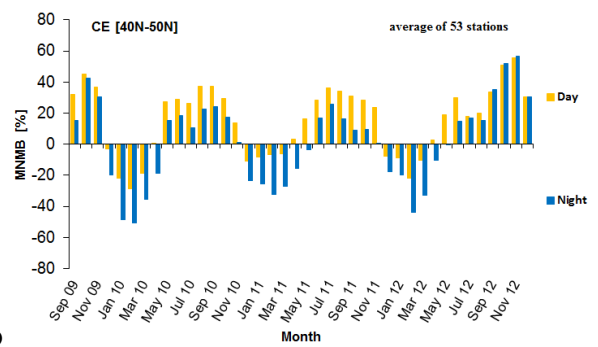
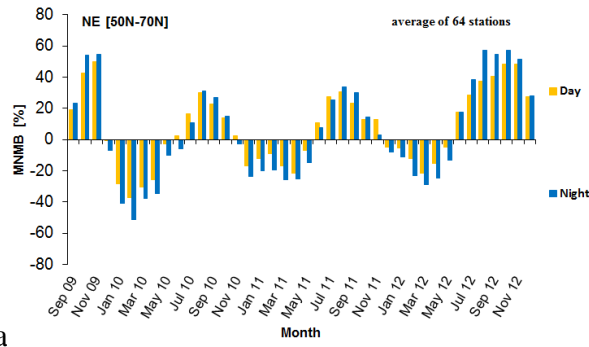
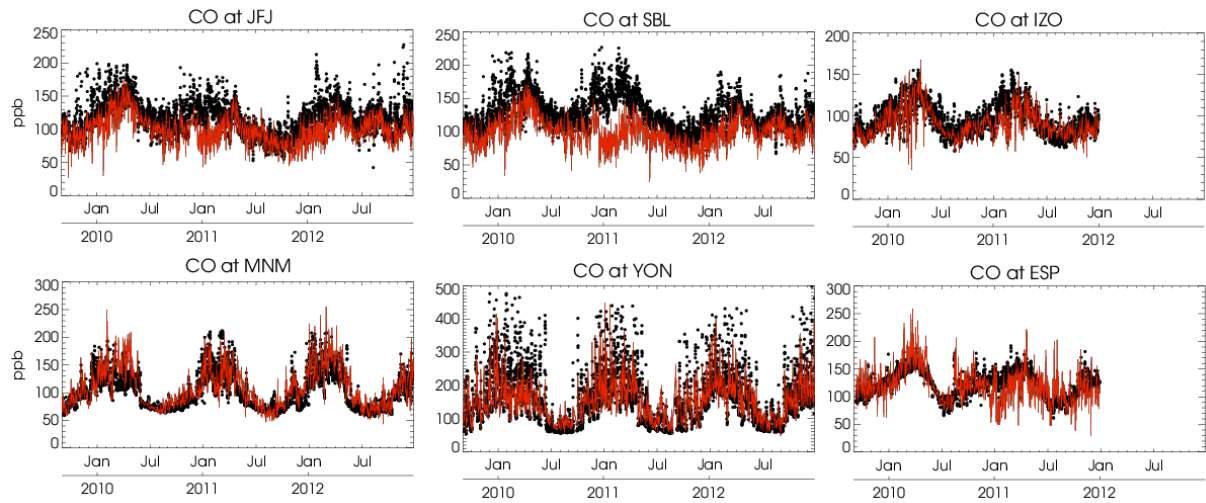
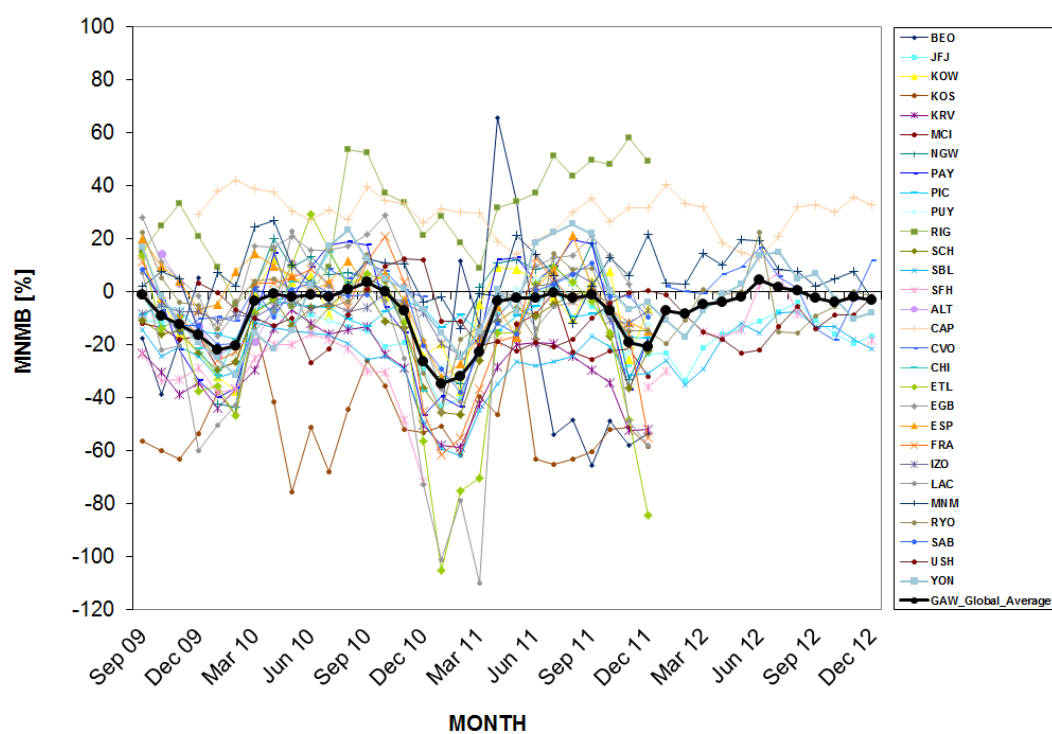


Figure 8: Modified normalized mean biases (MNMBs) derived from the evaluation of the MACC_osuite with EMEP O₃ surface observations during day-time (yellow color), and night-time (blue color) over northern Europe (a), central Europe (b) and southern Europe (c) during the period September 2009 to December 2012.



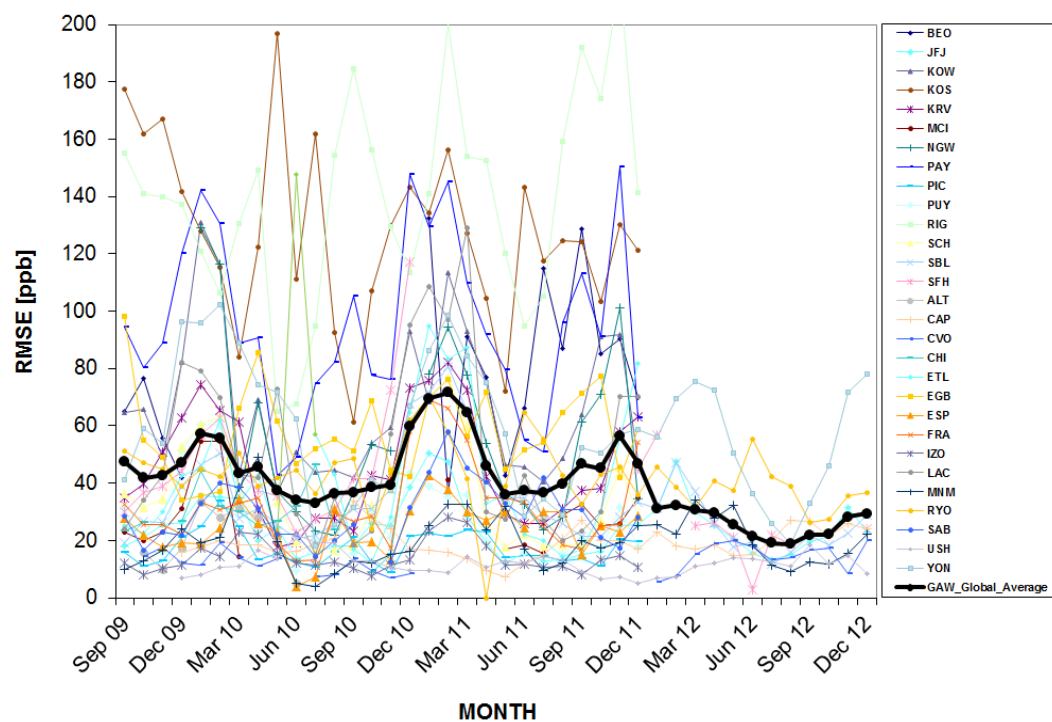
1
2 Figure 9: Time series plots of the MACC_osuite 6-hourly CO mixing ratios (red) and GAW
3 surface observations (black) for Jungfraujoch- JFJ (Switzerland), Sonnblick- SBL (Austria),
4 Izana Observatory- IZO (Tenerife), Minamitorishima- MNM (Japan), Yonagunijima- YON
5 (Japan) and Estevan Point- EVP (Canada) during the period 09/2009 to 12/2012. Unit: ppb.

1



2

3 Figure 10: Modified normalized mean bias (MNMB) in % derived from the evaluation of the
 4 MACC_osuite with GAW CO surface observations over the period September 2009 to
 5 December 2012 (black line: global average of 29 GAW stations. Multi-coloured lines:
 6 individual station results, see legend to the right).



1
2 Figure 11: Root mean square error (RMSE) in ppb derived from the evaluation of the
3 MACC_osuite with GAW CO surface observations over the period September 2009 to
4 December 2012 (black line: global average of 29 GAW stations multi-coloured lines:
5 individual station results, see legend to the right).

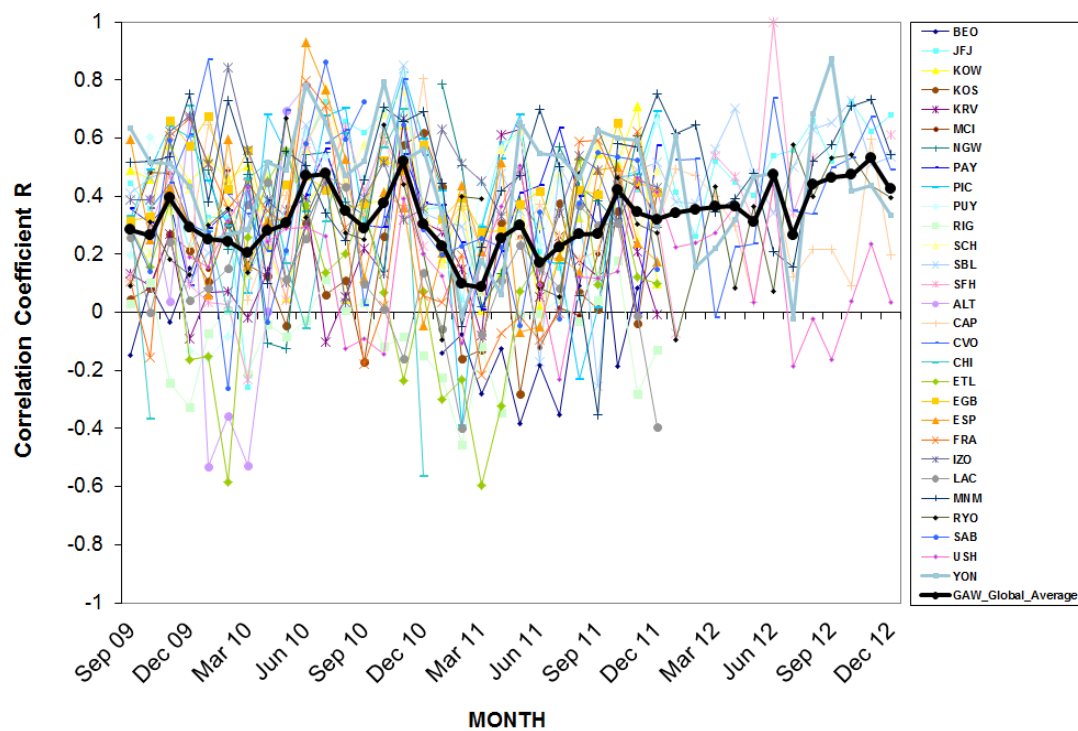
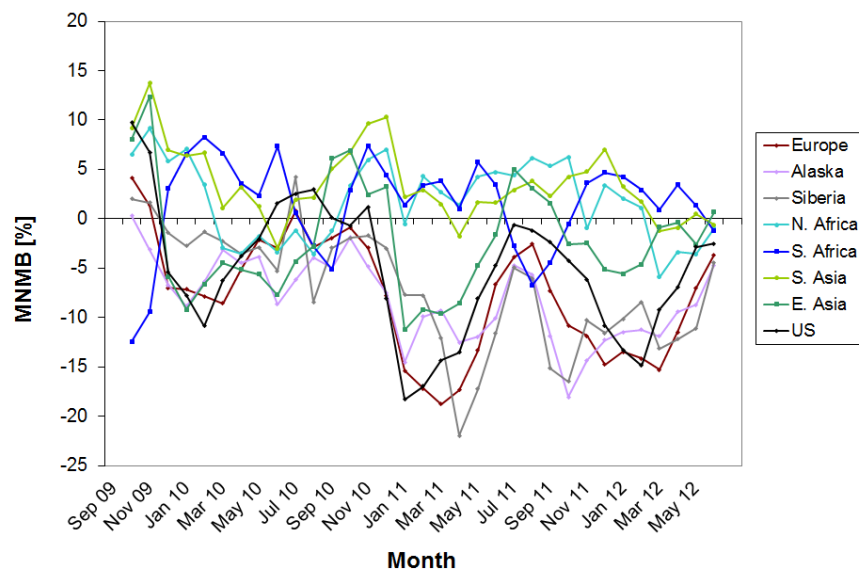


Figure 12: Correlation coefficient (R), derived from the evaluation of the MACC_osuite with GAW CO surface observations over the period September 2009 to December 2012 (black line: global average of 29 GAW stations. Multi-coloured lines: individual station results, see legend to the right).



1
2 Figure 13: Monthly average of modified normalized mean biases (MNMBs) derived from the
3 comparison of the MACC_osuite with MOPITT CO total columns for 8 different regions
4 during the period 09/2009 to 06/2012 (see legend on the right).

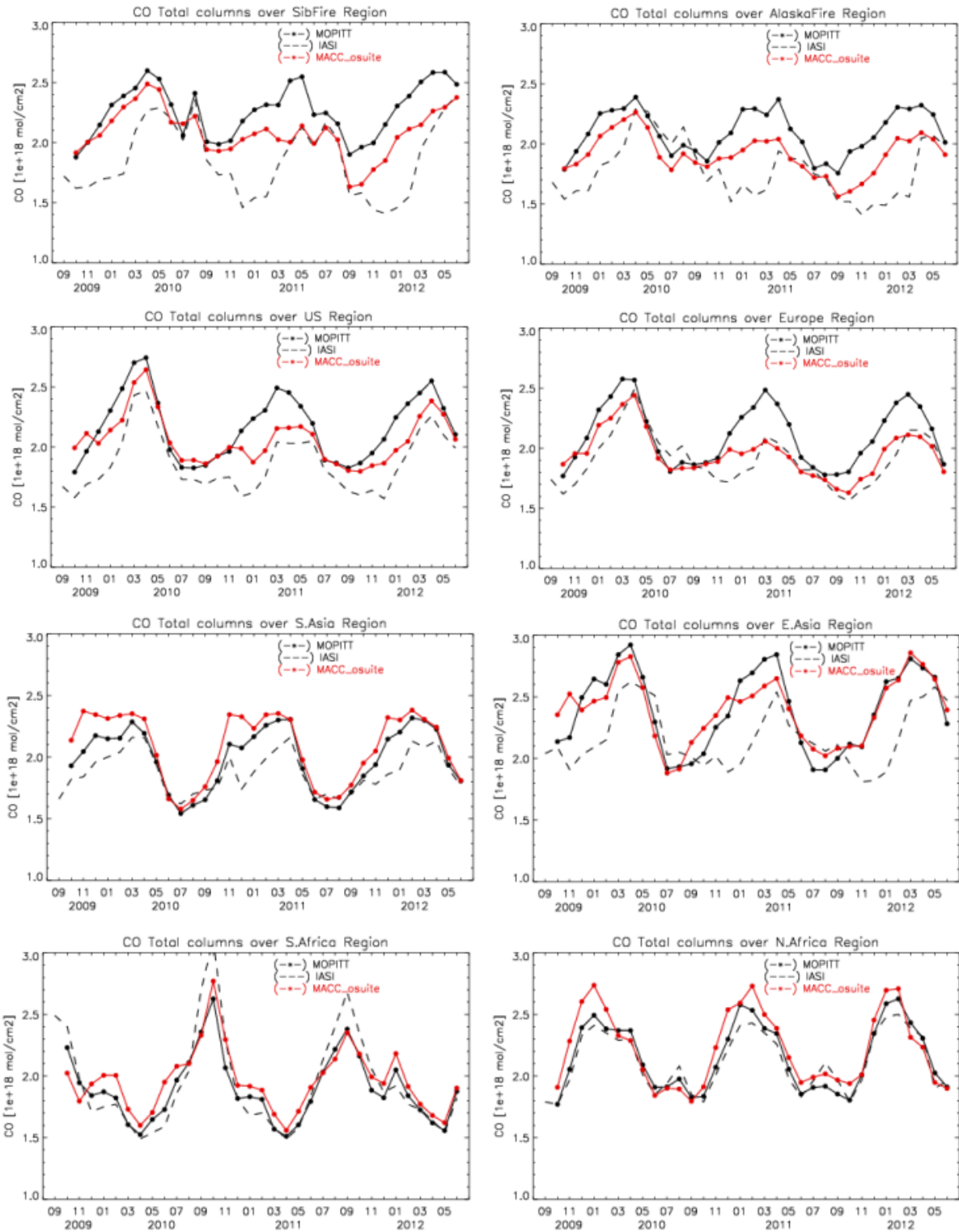
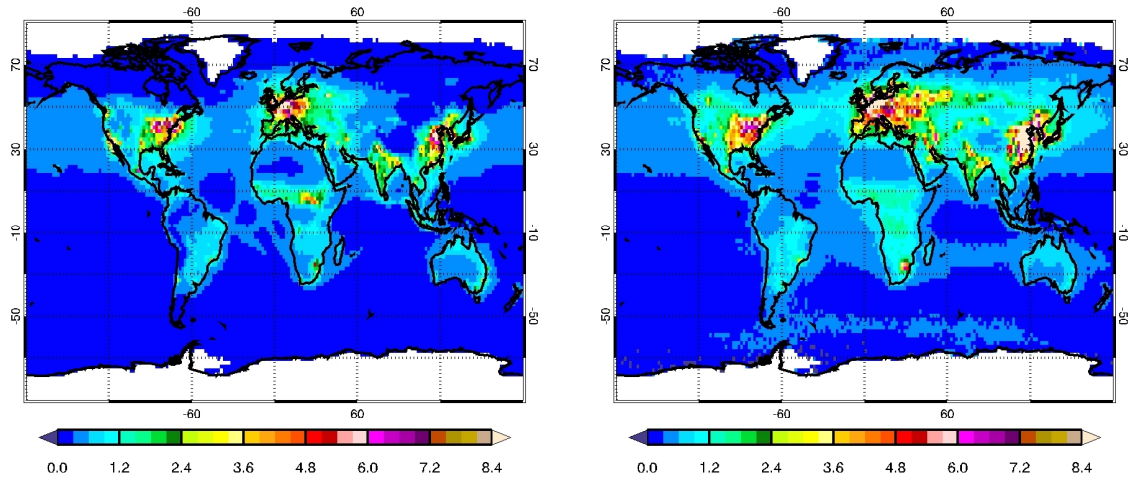
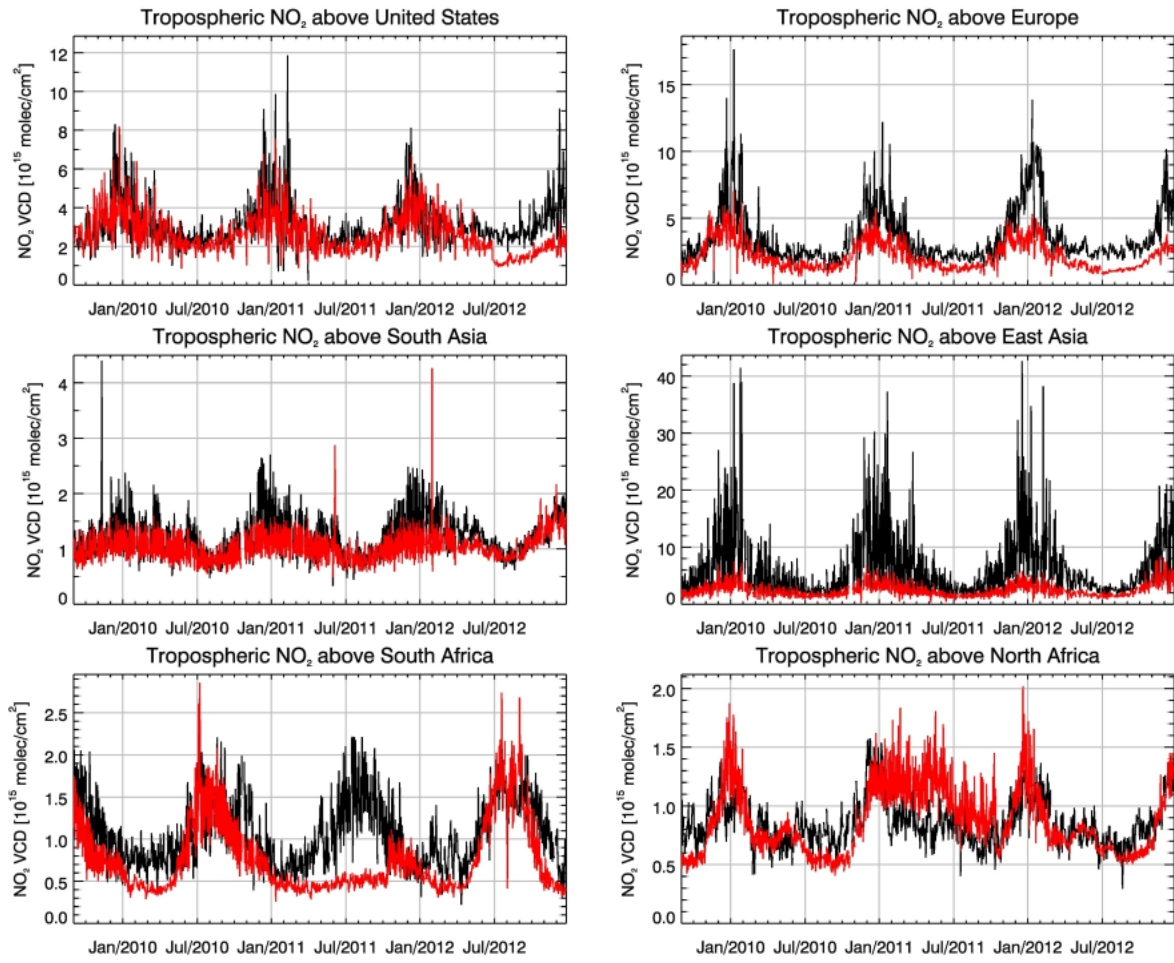


Figure 14: Time series plots of MOPITT CO total columns (black line) compared to IASI CO total columns (black dashed line) and the MACC_osuite CO total columns (red line) for 8 different regions (defined in Figure 1) during the period 09/2009 to 06/2012. Top: Siberia (left), Alaska (right), second row: United States (left), Europe (right), third row: South Asia (left), East Asia (right) bottom: South Africa (left), North Africa (right).



1
2 Figure 15: Long-term average of daily tropospheric NO₂ VCD [10^{15} molec cm⁻²] from
3 September 2009 to March 2012 for (left) MACC_osuite simulations and (right)
4 SCIAMACHY satellite observations. Blue colours represent low values; red/brown colours
5 represent high values.

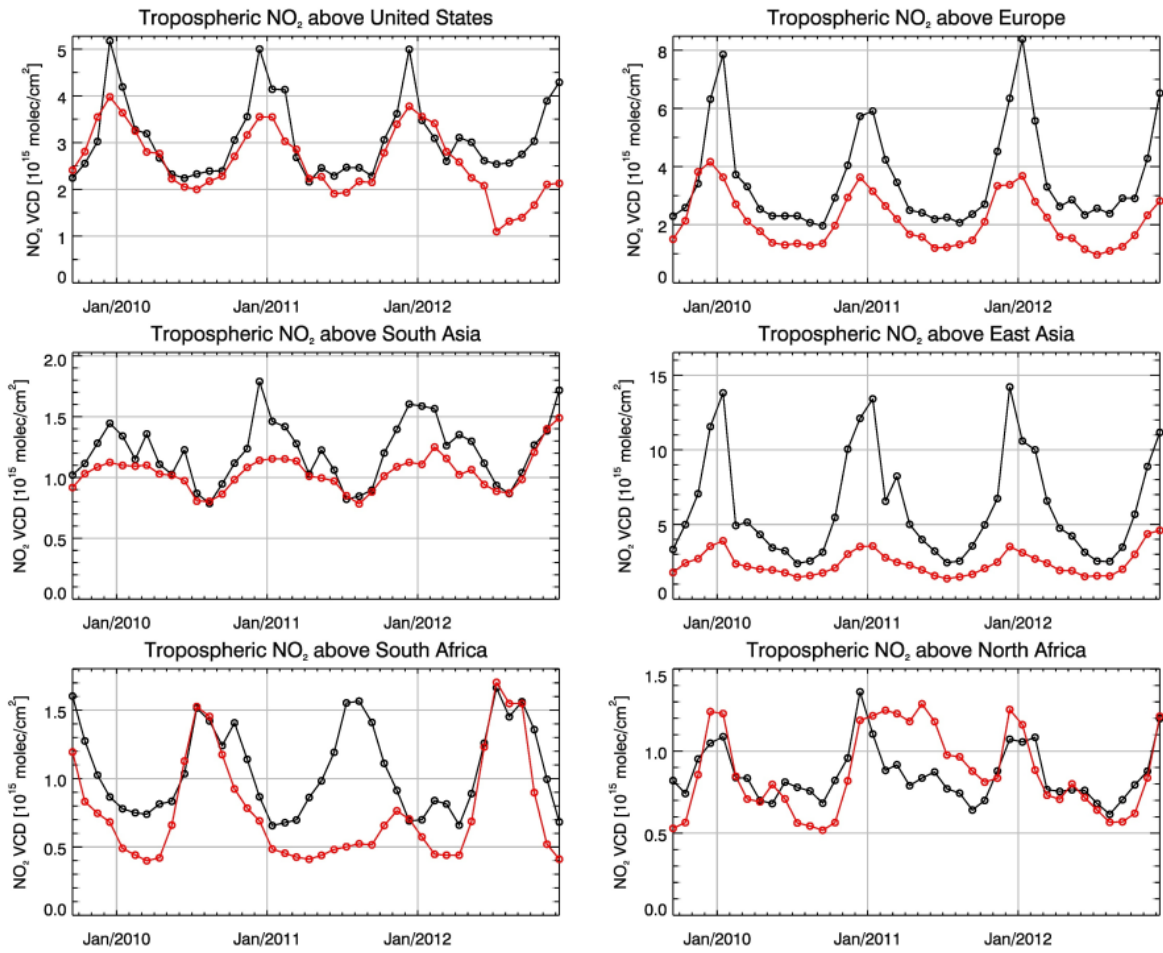
1



2

3 Figure 16: Time series of daily tropospheric NO₂ VCD [10^{15} molec cm⁻²] averaged over
 4 different regions. Top: United States (left), Europe (right), second row: South Asia (left), East
 5 Asia (right), bottom: South Africa (left), North Africa (right). Black lines show satellite
 6 observations (SCIAMACHY up to 03/2012, GOME-2 from 04/2012 to 12/2012), red lines
 7 correspond to the MACC_osuite simulations.

8



1
2 Figure 17: As in Fig. 16 but for monthly means of daily tropospheric NO₂ VCD [10^{15} molec
3 cm^{-2}] averaged over different regions. Top: United States (left), Europe (right), second row:
4 South Asia (left), East Asia (right), bottom: South Africa (left), North Africa (right).

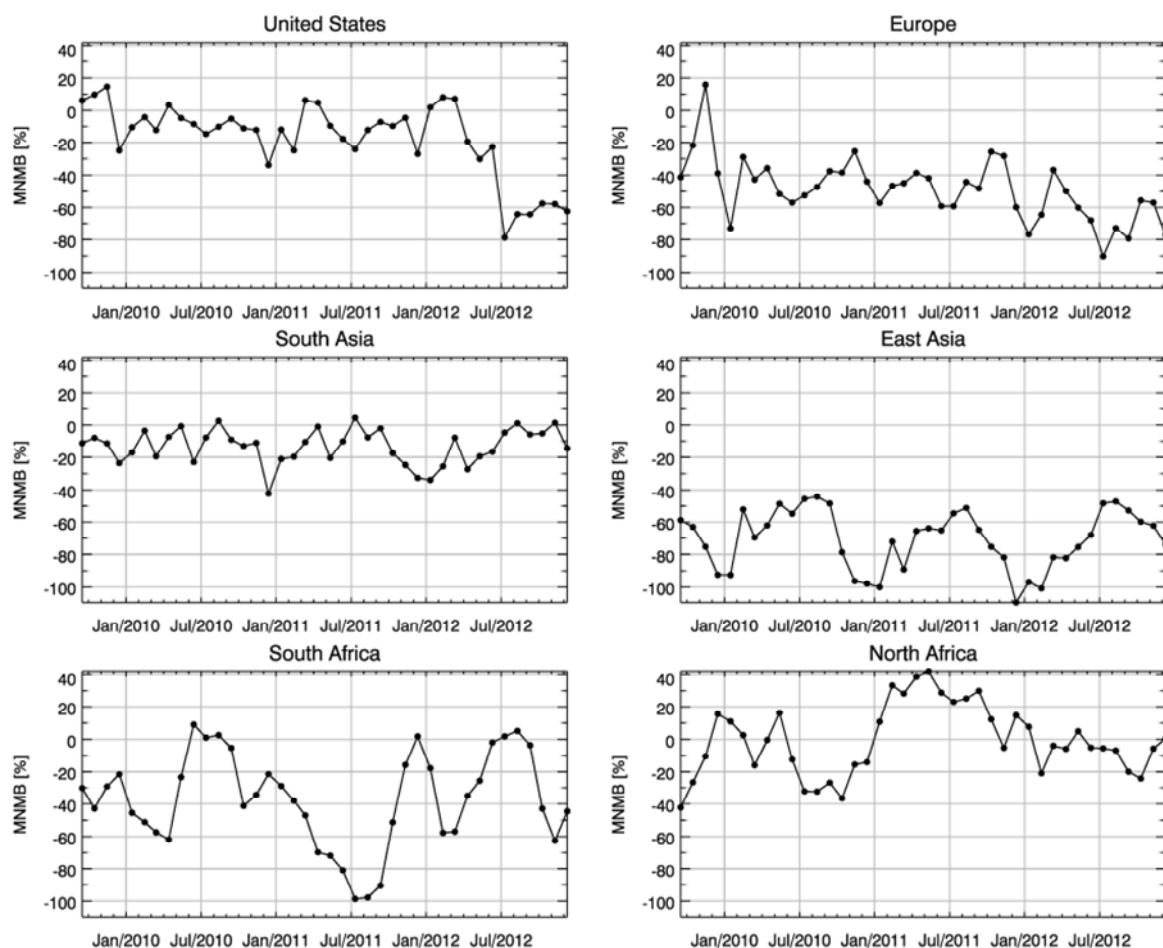
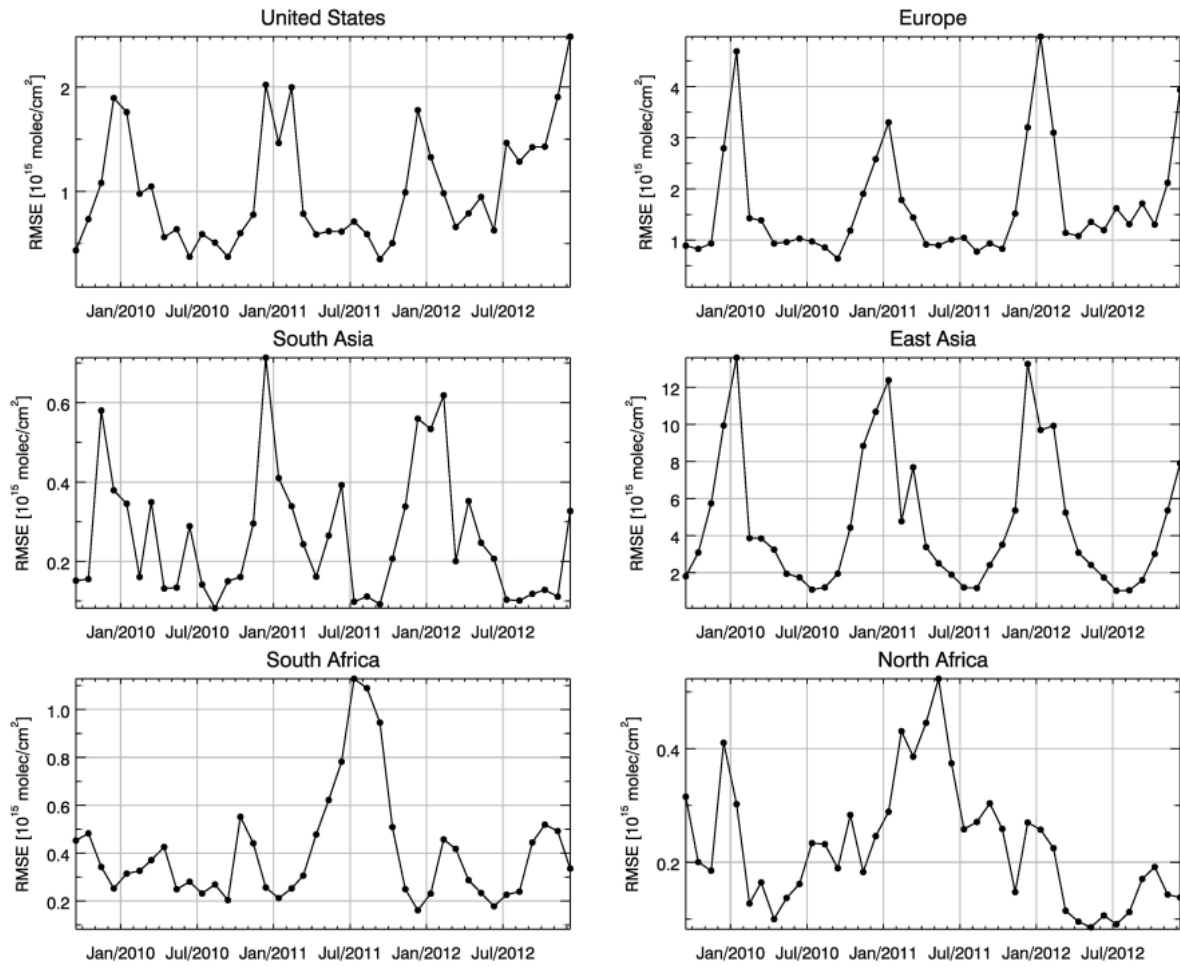


Figure 18: Modified normalized mean bias [%] for monthly means of daily tropospheric NO₂ VCD averaged over different regions (see Fig.1 for latitudinal and longitudinal boundaries) derived from the MACC_osuite simulations and satellite observations (SCIAMACHY up to 03/2012, GOME-2 from 04/2012 to 12/2012). Top: United States (left), Europe (right), second row: South Asia (left), East Asia (right), bottom: South Africa (left), North Africa (right). Values have been calculated separately for each month.



1

2 Figure 19: As in Fig. 18 but for the root mean square error [10^{15} molec cm⁻²].

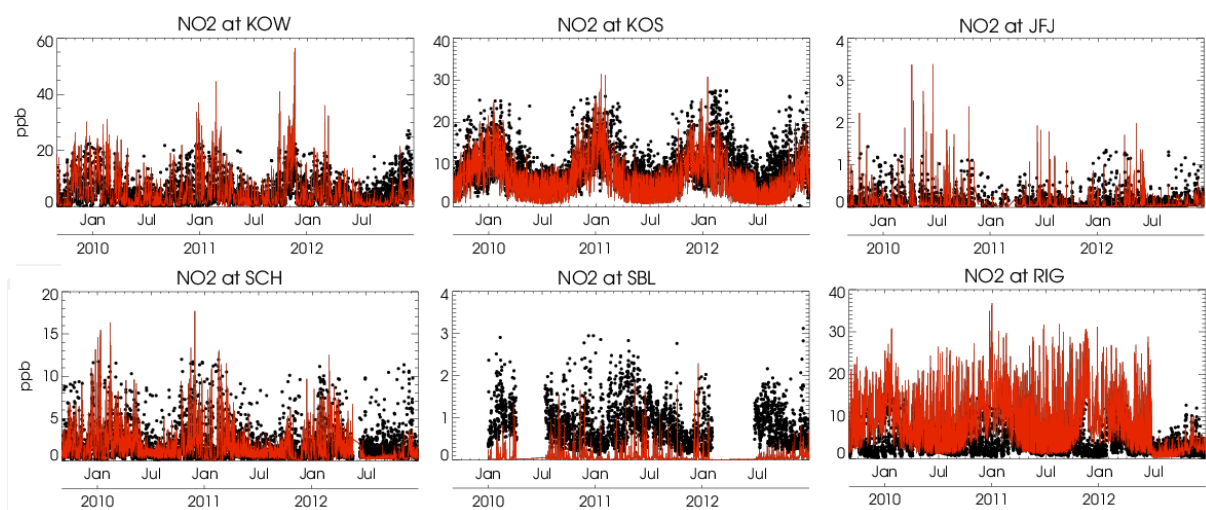
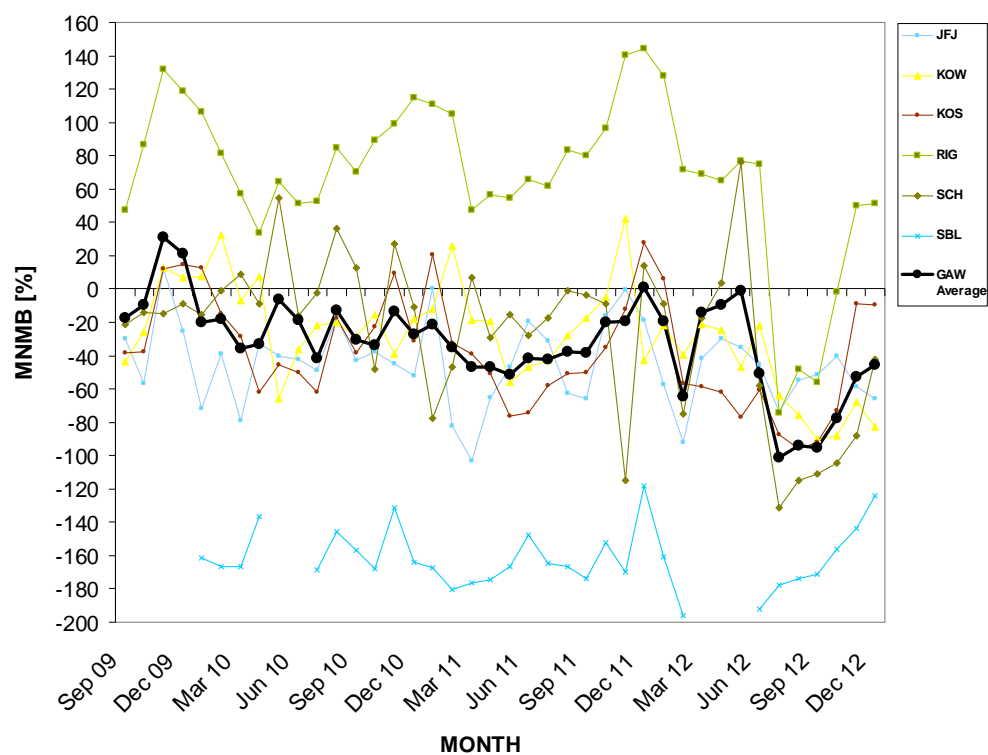
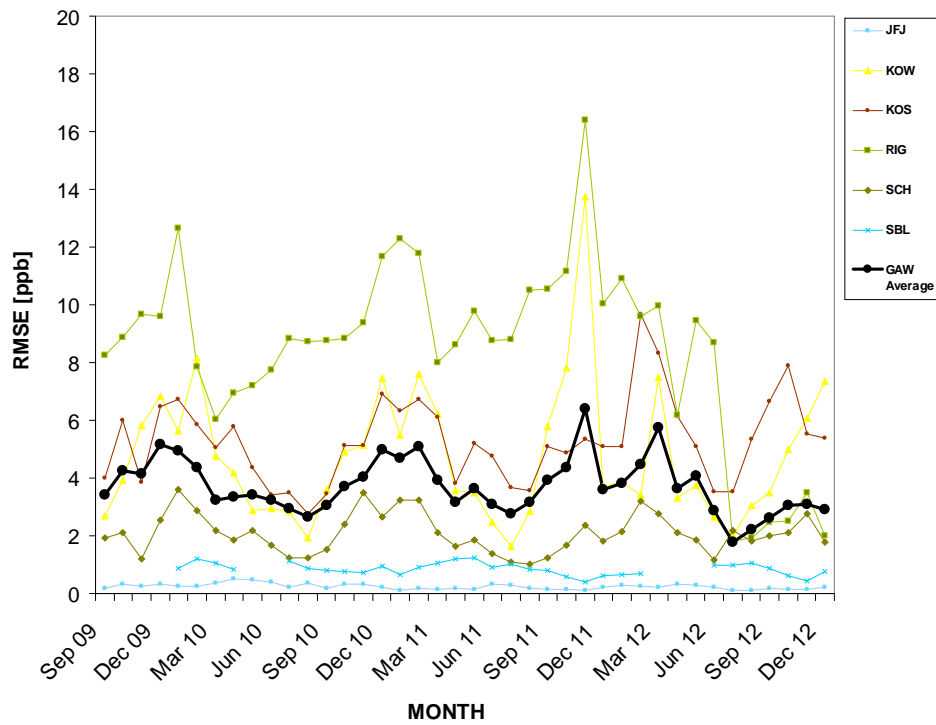


Figure 20: Time series plots of the MACC_ensemble 6-hourly NO₂ mixing ratios (red) and GAW surface observations (black) for Kollumerwaard- KOW (Netherlands), Kosetice-KOS (Czech Republic), Jungfraujoch- JFJ (Switzerland), Schauinsland-SCH (Germany), Sonnblick- SBL (Austria) and Rigi-RIG (Switzerland) during the period 09/2009 to 12/2012. Unit: ppb.



1
2 Figure 21: Modified normalized mean bias (MNMB) in % derived from the evaluation of the
3 MACC_osuite with GAW NO₂ surface observations over the period September 2009 to
4 December 2012 (black line: global average of 6 GAW stations. Multi-coloured lines:
5 individual station results, see legend to the right).



1
2 Figure 22: Root mean square error (RMSE) in ppb derived from the evaluation of the
3 MACC_osuite with GAW NO₂ surface observations over the period September 2009 to
4 December 2012 (black line: global average of 6 GAW stations multi-coloured lines:
5 individual station results, see legend to the right).

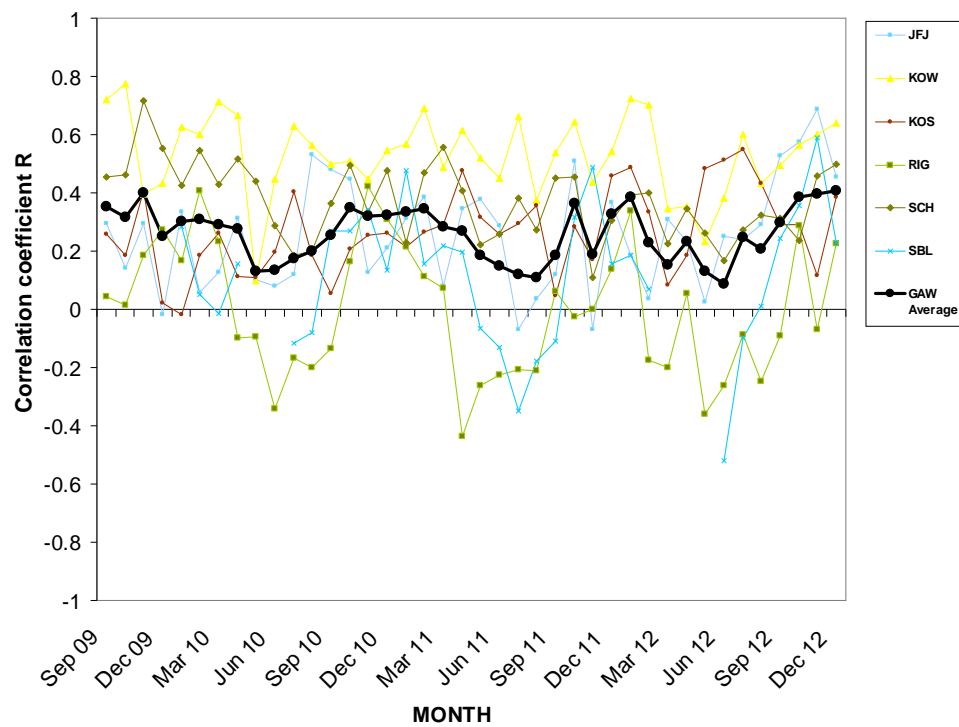


Figure 23: Correlation coefficient (R), derived from the evaluation of the MACC_osuite with GAW NO₂ surface observations over the period September 2009 to December 2012 (black line: global average of 6 GAW stations. Multi-coloured lines: individual station results, see legend to the right).